To the Graduate Council:

I am submitting herewith a thesis written by Glen Arthur Kroeger entitled "Anode Current Distribution on a Diagonal Conducting MHD Generator." I recommend that it be accepted in partial fulfillment of the requirements for the degree of Master of Science, with a major in Physics.

J. B. Dicks

John B. Dicks, Jr., Major Professor

We have read this thesis
and recommend its acceptance:

D M Mason

Ying-chu Lin Wu

Accepted for the Council:

Hilton A. Smith

Vice Chancellor
Graduate Studies and Research

# ANODE CURRENT DISTRIBUTION ON A DIAGONAL CONDUCTING MHD GENERATOR

A Thesis

Presented for the

Master of Science

Degree

The University of Tennessee, Knoxville

Glen Arthur Kroeger

June 1976

1286598

## ABSTRACT

A method for measuring current distribution in two dimensions simultaneously in a 60-degree diagonal conducting wall generator is devised and tested. The measurements of current density are made in the direction longitudinal and transverse to the plasma flow. Segmentations of the surface are 1.8 mm by 5.5 mm made on a solid block of Inconel 625. The high resistivity of this alloy provides a signal of 100 microvolts for a current density of 1 amp/cm$^2$. Both current and temperature are measured on selected segments. Temperatures at the plasma-electrode interface and one cm beneath the surface are recorded. Comparison of current distribution measurements with theory in the longitudinal direction is made.

TABLE OF CONTENTS


| CHAPTER | | PAGE |
|---|---|---|
| I. | INTRODUCTION | 1 |
| | Literature Review | 1 |
| | Generator Physics | 5 |
| | Current Density Equations | 7 |
| II. | DESCRIPTION OF EXPERIMENTS | 11 |
| | Experimental Facility | 11 |
| | Design of the Electrode | 13 |
| | Electrode Material | 13 |
| | Electrode Segmentation | 15 |
| | Electrode Nomenclature | 15 |
| | Electrode Instrumentation | 17 |
| | Electrode Cooling | 22 |
| | Electrode Fabrication | 23 |
| | Vidar System Instrumentation | 25 |
| | Grounding and Noise Effects | 25 |
| | Calibration of the Electrode | 28 |
| | Thermal Effect on Resistivity | 32 |
| | Run Procedure | 32 |
| III. | DISCUSSION OF DATA | 36 |
| | Synopsis of the Tests | 36 |
| | Discussion of Data on Run Number 1482 | 37 |
| | Discussion of Data on Run Number 1483 | 47 |
| | Discussion of Data on Run Number 1487 | 52 |

CHAPTER PAGE

Comparison with Conformal Mapping Theory . . . . 62

IV. CONCLUSIONS AND RECOMMENDATIONS. . . . . 66

BIBLIOGRAPHY . . . . . 68

VITA . . . . . 71

LIST OF FIGURES


| FIGURE | | PAGE |
|---|---|---|
| 1. | Current Distribution Model and Channel Geometry. . . . . | 8 |
| 2. | Location of the Test Electrode in the Experimental Facility . . . . . | 12 |
| 3. | The Segmented Electrode After the Installation of the Instrumentation. . . . . | 14 |
| 4. | Instrumented Segments of the Testing Electrode . . . . . | 16 |
| 5. | Location of All Instrumentation as Viewed at the Plasma-Inconel Interface. . . . . | 18 |
| 6. | Shielding of Instrumentation Wires. . . . . | 27 |
| 7. | Positions of Nonequipotential on the Electrode Surface with Current Applied at the Center Point. . . . . | 29 |
| 8. | Generator Multiload Configuration . . . . . | 33 |
| 9. | Two-terminal Load Configuration with Relays for Load Switching. . . . . | 35 |
| 10. | Load Line Curves for Tests that Produced Measurable Power. . . . . | 38 |
| 11. | Temperature versus Time Plot of Surface Type S Thermocouples on Run Number 1482. . . . . | 40 |
| 12. | Temperature History of Segments for Run Number 1482 . . . . . | 41 |
| 13. | Current Density and Hall Voltage on C4 and A4 Segments Plotted versus Time for Run Number 1482 . . . . . | 42 |
| 14. | Temperature and Current Density History of Segments on Run Number 1482 . . . . . | 43 |
| 15. | Histogram of Initial Cathodic Behavior on the Collecting Electrode for Run Number 1482. . . . . | 45 |

FIGURE PAGE

16. Current Density and Hall Voltage for Run Number 1482 Plotted versus Time when Magnetic Field is Turned Back On. . . . . 46

17. Current Density versus Time for Segments on Run Number 1483 . . . . . 49

18. Current Histogram Showing the Mean, Standard Deviation, and Deviation in the Mean Taken for Each Data Set for Run Number 1483 . . . . . 50

19. Time-Averaged Current Density for Each Segment and at Each Load on Run Number 1483 . . . . . 51

20. Temperature History of Run Number 1483. . . . . 53

21. Current Density Histogram for Segments on Run Number 1487 . . . . . 54

22. Current Density Histogram with B3 Segment Read Several Times During Each Data Set for Run Number 1487 . . . . . 56

23. Time-Averaged Current Density on Run Number 1487 for Each Segment and Load . . . . . 57

24. Time-Averaged Current Density as a Function of Position for Run Number 1487 at 10-ohm Load . . . 59

25. Time-Averaged Current Density as a Function of Position for Run Number 1487 at 6-ohm Load. . . . 60

26. Time-Averaged Current Density as a Function of Position for Run Number 1487 at Zero-ohm Load. . . . . 61

27. Comparison of Experimental and Theoretical Current Distribution on the Anode on Run Number 1487 and at 10Ω Load . . . . . 65

# CHAPTER I

# INTRODUCTION

It has been found both theoretically and experimentally that current flow from MHD electrodes is not always uniformly distributed. This experiment has been conceived to measure current distribution in the direction longitudinal and transverse to the gas flow. It is known that current also flows to the side walls. The experiment has been designed to measure current on a testing electrode mounted on the bottom side of the generator which is the anode under normal magnetic field orientation. However, the testing electrode acts as a cathode when the magnetic field direction is reversed. The instrumented electrode is an integrated part of a 60-degree diagonal conducting wall (DCW) MHD generator.

The principle of measurement was to obtain the voltage drop across Inconel segments having dimensions of 1 cm by 0.18 cm by 0.55 cm. One milliamp through a segment produces about one microvolt. One hundred microvolts corresponds to approximately 1 amp/$cm^2$.

## Literature Review

There has been considerable interest in current density and current distribution in MHD generators for some time. Both theoretical and experimental studies have been

made in two dimensions only. The present study has been undertaken to develop the technique and obtain data for current distribution in the plane of an anode electrode where longitudinal and transverse measurements are made simultaneously. Previously, the segmentation of an electrode has been only in one direction, either in the flow direction or the magnetic field direction.

An early theoretical study on an MHD generator by Hurwitz, Sutton, and Kilb [1][1] obtained current distribution in the flow direction on perfectly conducting Faraday electrodes. It was shown that current tended to concentrate on the upstream edge of the anode and the downstream edge of the cathode when the conductivity was assumed uniform and the insulators infinitely nonconducting. Finite longitudinal segmentation of the electrodes and the Hall effect are the cause of this concentration. Later, Oliver and Mitchner [2] introduced a step variation in electrical conductivity. It was shown that current concentration increases when the conductivity directly above an electrode increases. Similarly, current is more uniform when the conductivity is reduced. Joulean heating occurs where the current concentrates, as would be expected.

S. T. Demetriades, et al., [3] have reported experimental and theoretical results similar to Oliver. Current

---

[1]Numbers in brackets refer to similarly numbered references in the bibliography.

concentrations are diminished by a resistive layer. Further, according to their results, cold wall generators are able to produce power only if Joule heating increases the temperature of the resistive layer above a critical level. Experimentally it was found that a current density of 3.2 amps/$cm^2$ caused rapid erosion of uncoated copper and Inconel electrodes. The temperature of the surface was below 900 C. For the Avco Everret Mark VI channel, computer simulations indicate that current concentrations of 7 amps/$cm^2$ are possible. When the Inconel and copper electrodes were coated with a layer of zirconia, no erosion was observed on the zirconia in the Demetriades tests. However, chemical erosion occurred at the Inconel-zirconia interface.

Several previous studies of current distribution have been made at The University of Tennessee Space Institute (UTSI). A study of a Faraday generator by Taylor, et al., [4] with more realistic gasdynamic properties showed that current distribution is sensitive to the type of boundary and wall temperature. For a wall temperature of 1,500 K, $\delta$ = 0.1 h, and $M_\infty$ = 1.5, the current distribution is quite uniform. $\delta$ is the thickness of the boundary layer and $M_\infty$ is the free stream Mach number. If the wall temperature is held constant and $\delta$ and $M_\infty$ are changed, current distribution does not vary more than 15%. A wall temperature of 2,700 K, however, has current distributions varying 30% for a laminar boundary layer

profile. Current distributions vary 80% to 100% for turbulent profiles as $\delta$ and $M_\infty$ are changed.

Experimental work by Nicholson [5] has shown axial current nonuniformities in a diagonal conducting wall generator. In three-dimensional measurements, the anode always carried more current in the center of the generator. As the load is increased the anode current tends to shift upstream. Upstream current was about twice the downstream current for a 30-ohm load. At short circuit, however, his data shows about 25% less current upstream than downstream. Side wall looping current at high Hall fields follows the same trend in axial nonuniformity. The current density is of the order of 0.5 amp/cm$^2$ on the anode and 0.2 amp/cm$^2$ on the side wall without looping. The current density increases steadily as the Hall field increases.

Experimental work by Martin [6] was undertaken to study the current distribution in the cross-sectional plane of a Hall generator using a segmented electrode. Several test configurations were used to show their effect on the current distribution. Ten segmentations were made transverse to the plasma flow. The open circuit distribution varied from 0.3 amp/cm$^2$ at the edges to 1.5 amps/cm$^2$ in the center of the electrode. Side wall current averaged 1 amp/cm$^2$ on one side and 0.6 amp/cm$^2$ on the other. Changing the load to short circuit changed the anode current only slightly. For these tests, five segments each 0.25-cm wide were made on the side walls. Ten segments 0.5-cm wide

comprised the anode. The channel was of the heat sink type so all runs were short (approximately 13 seconds).

Stephans [7] did similar work on a 60-degree DCW generator. It was found that current distribution for this case was similar to the Hall channel. Also, a larger anode voltage drop forces more current to the side walls. The data from Stephans shows that the anode current distribution for high side wall current (76%) is essentially uniform at 0.1 amp/$cm^2$. The channel was in the short circuit mode. When a 5-ohm load was applied, current varied from 1.0 amp/$cm^2$ on the edge to 2.3 amps/$cm^2$ in the center. Side wall current for this case was 65%. At a 10-ohm load, the current was uniform at 2 amps/$cm^2$ with a side wall current of 60%. A 13.3-ohm load produced 80% side wall current at slightly less than 1 amp/$cm^2$. It is interesting to note that the total power output of the generator follows the percent of current flowing on the side walls. More power is produced when the side wall current is reduced. For instance, a power level of 22.2 KW had 70% anode side wall current; a 33.6-KW level had 43% wall current; and a level of 36 KW had 41% side wall current. However, due to non-uniformities, the generator performance is degraded if the side walls are made insulating [5].

## Generator Physics

From Steenbeck's minimum principle [8] it is known that each time an electrical discharge has a choice of

paths, it will choose the path of least voltage drop. The MHD generator is an excellent example of discharge coupling and discharge path selection. Nicholson [5] has pointed out that cathode current on a single electrode is roughly constant. That is, when current on one part of a divided cathode goes up, current on another part goes down. Muehlhauser [9] similarly has concluded that the average number of cathode arc spots per electrode in a DCW generator is two; he observed their appearance and disappearance in pairs.

Thus far, no specific analysis has been made on the coupling between the anode and cathode conduction on a particular electrode. Existing data may shed some light on this facet of the conduction problem for DCW generators, but no experiment has been designed with this in mind. Certainly, for the class of conducting wall generators, the anode and cathode must conduct nearly simultaneously. If this were not so, the charge build-up or depletion would soon prohibit any further conduction. An exception to this would be for those electrodes used as power terminals. Since the conduction processes and voltage drop losses are different for cathode and anode [5], this makes a very interesting fluctuation about equilibrium problem.

Viewing the generator as a whole, the electrodes are coupled to each other through the plasma, and Steenbeck's principle applies. That is, electrodes conduct according to the local plasma potential and are influenced by conduction

on nearby electrodes. Because of the $\vec{v} \times \vec{B}$ force on the electrons, they are forced to orbit at their cyclotron radius. The electrons would be stopped in their average translational velocity if it were not for the ions dragging them on to maintain plasma neutrality. Nevertheless, the electrons' resistance to the motion through the magnetic field produces the Hall effect voltage. Thus, there is a slight average separation of the negative and positive charges. In addition, the electrons have a net transport toward the anode because the probability of a scattering collision is greater traveling against the gas flow than with it during the cyclotron orbit.

Current Density Equations

Two-dimensional current distribution, as shown in Figure 1, with segmentation in the x-direction has been discussed by Muehlhauser [9] using conformal mapping methods. His treatment is a modification of the work by Wu, et al., [10] in that the cathode current conduction is no longer considered uniform. Denzel, et al., [11] has calculated the current density on the electrodes to be given by the following equation:

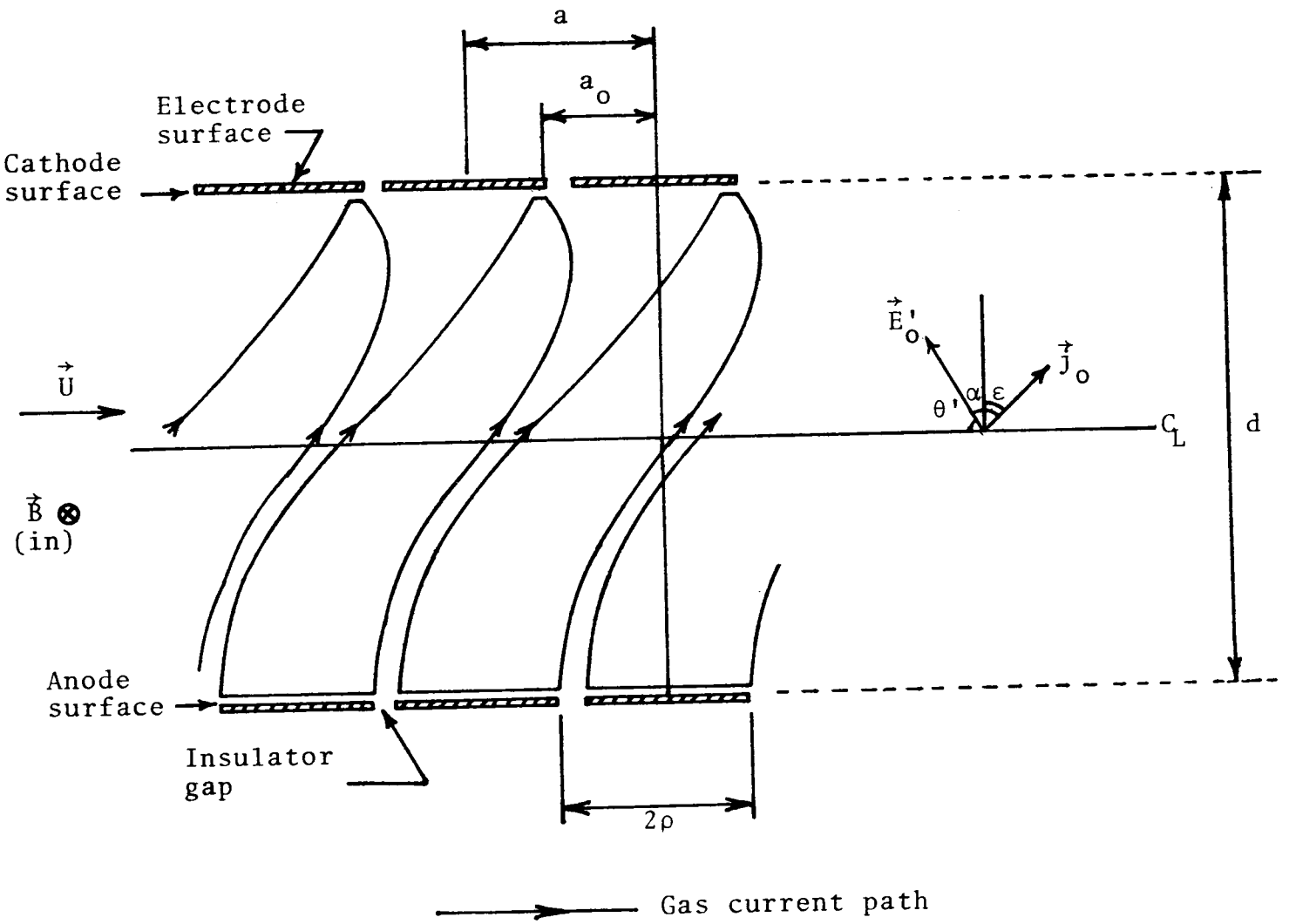



Figure 1. Current distribution model and channel geometry.

$$j_x - ij_y = \frac{I_E}{A\,\frac{2\rho}{d}\cos\varepsilon}\left\{\frac{\cos(\pi c(1-k)-\varepsilon)}{\sin \pi c}\left[\frac{\sin\frac{\pi}{2\rho}z}{\sin\pi(c'-\frac{z}{2\rho})}\right]^{-k}\right.$$

$$\left. - \frac{\cos(\pi ck+\varepsilon)}{\sin \pi c}\left[\frac{\sin\frac{\pi}{2\rho}z}{\sin\pi(c'-\frac{z}{2\rho})}\right]^{1-k}\right\}, \qquad (1)$$

where $\alpha = \tan^{-1}\Omega$; $k = \frac{1}{2} - \frac{\alpha}{\pi}$; $z = x + iy$; and $c' = 1 - c$. Cos $\varepsilon$ is part of the generator operation parameter to be defined later. Figure 1 shows $2\rho$ and d. $\Omega$ is the Hall parameter, and $\alpha$ is the angle between the electric field and the current in the generator far away from the electrodes. For this analysis it was assumed that the current was uniform in the center of the generator. c' is defined as the normalized insulator width and c is the normalized electrode width.

The current from one electrode is given in [13] by

$$I_E = \frac{2\rho\sigma UBD\left[1-\frac{V_a+V_c}{UBd}\right]}{(\frac{a_o}{d}+\frac{2\rho}{d}u')(\Omega-\tan\varepsilon)+(1+\tan\varepsilon)(1+\frac{2\rho}{d}v')}, \qquad (2)$$

where D is the width of the channel normal to the flow and perpendicular to the magnetic field. The generator operation parameter, tan $\varepsilon$, from [9] is given by

$$\tan \varepsilon = \frac{(\frac{a_o}{d} - \frac{2\rho}{d} u) - \frac{I}{\sigma UBA(1-\Delta)}[(1 + \Omega \frac{a_o}{d}) + \frac{2\rho}{d}(v' + \Omega u')]}{\frac{I}{\sigma UBA(1-\Delta)}[\Omega - \frac{a_o}{d} + \frac{2\rho}{d}(\Omega v' - u')] - (1 + \frac{2\rho}{d} v)} , \qquad (3)$$

where $\Delta = \frac{V_a + V_c}{UBd}$ , the loss parameter due to voltage drop across the anode and cathode sheath; I is the total generator current; u', v', u, and v are complicated integrals evaluated by Denzel for this particular geometry; $a_o$ is as shown in Figure 1, page 8; $\sigma$, U, B, and A are the plasma conductivity, gas flow velocity, magnetic field, and area normal to the flow, respectively.

From Eq. (1) it can be shown [9] by separating the real and imaginary parts that

$$j_y = -j_o[C \sin(-k\pi)R^k + D \sin(1-k)\pi R^{k-1}] , \qquad (4)$$

where

$$j_o = \frac{I_E}{\frac{2\rho}{d} A \cos \varepsilon} ; \quad C = \frac{\cos[\pi c(1-k) - \varepsilon]}{\sin \pi c} ; \quad D = \frac{-\cos(\pi ck + \varepsilon)}{\sin \pi c} ;$$

and $R = [A'^2 + B'^2]^{1/2}$. The terms under the radical are

$$A' = \frac{(A_1 C_1 + B_1 D_1)\sin \pi c'}{C_1^2 + D_1^2 - \cos \pi c'} \text{ and } B' = \frac{(B_1 C_1 - A_1 D_1)\sin \pi c'}{C_1^2 + D_1^2} ,$$

where

$$A_1 = [e^{\frac{\pi y}{2\rho}} + e^{\frac{-\pi y}{2\rho}}]\cos \frac{\pi x}{2\rho} , \quad B_1 = [-e^{\frac{\pi y}{2\rho}} + e^{\frac{-\pi y}{2\rho}}] \sin \frac{\pi x}{2\rho} ,$$

$$C_1 = [e^{\frac{\pi y}{2\rho}} + e^{\frac{-\pi y}{2\rho}}]\sin \frac{\pi x}{2\rho} , \quad D_1 = [e^{\frac{\pi y}{2\rho}} - e^{\frac{-\pi y}{2\rho}}] \cos \frac{\pi x}{2\rho} .$$

# CHAPTER II

# DESCRIPTION OF EXPERIMENTS

## Experimental Facility

A fluidized coal/seed mixture is combined with oxygen in a combustor and burned to produce a plasma. The gas is expanded through a nozzle into a diverging diagonal conducting wall generator. From the generator the gas passes through a diffuser and is quenched with water in the exhaust duct. Figure 2 shows the location of the test electrode.

The entrance to the generator has dimensions of 5 cm by 10 cm and the exit is 5 cm by 30 cm. Overall length of the generator is 1.07 m. Each of the 71 electrodes is water-cooled. Insulation between electrodes is achieved by plasma spraying each electrode with alumina.

The magnetic field is provided by an electromagnet with pole pieces 0.914-m long. The pole gap has a constant width of 15 cm. Maximum strength is about 2 Telsa at a current of 1,600 amps.

At the location of the test electrode, 46 cm from the entrance to the generator, the plasma condition has the following nominal values: $p = 10.5$ psia; $T = 2{,}500$ K; $\sigma = 8.5$ mho/m; $\Omega = 1.7$; and $U = 1{,}390$ m/sec. These values are calculated by computer for a given power output of the generator. In this case the power is about 40 KW.

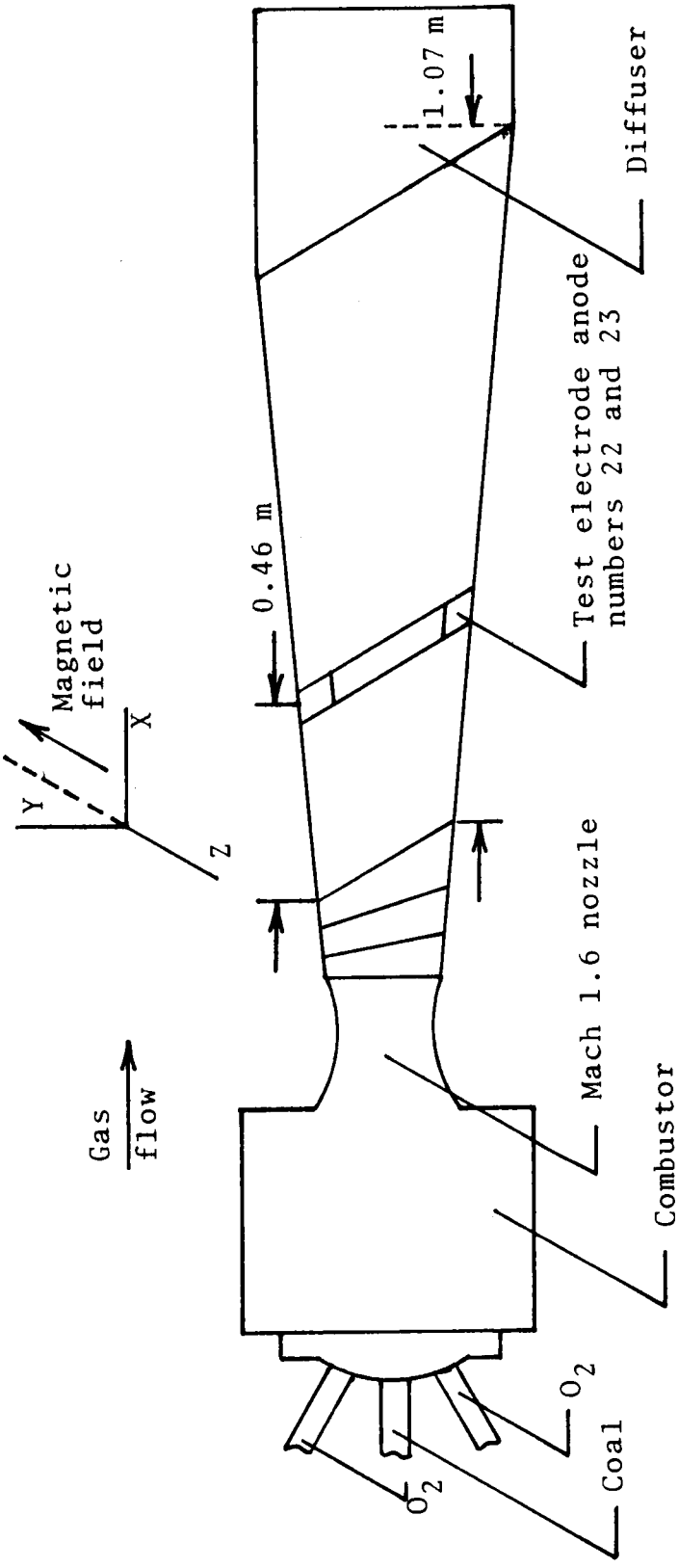



Figure 2. Location of the test electrode in the experimental facility.

## Design of the Electrode

The segmented electrode is part of a diagonal electrode with copper side walls. The anode in these experiments is determined by the direction of the magnetic field relative to the gas velocity. Therefore, the anode is on the bottom of the channel in the present arrangement. The velocity is in the positive x-direction and the magnetic field is in the negative z-direction.

The instrumented electrode for these current measurements is designed to perform as nearly as possible like a normal electrode. There are differences, however, which include the following: (1) the instrumented electrode is 2.54 cm wide instead of the normal 1.27 cm; (2) the anode portion is made of Inconel 625, while the side walls and top are of electrolytic copper; and (3) the Inconel portion had grooves machined to a depth of about 1 cm, each of which was filled with a slab of high density alumina. The segmented electrode was located at electrode numbers 22 and 23, about 46 cm from the entrance to the channel. Figure 3 shows the segmented electrode after the instrumentation was completed.

## Electrode Material

The material for the segmented electrode was chosen on the basis of high electrical resistivity, high thermal conductivity, high operating temperature capability, and high resistance to corrosion and intergranular attack.

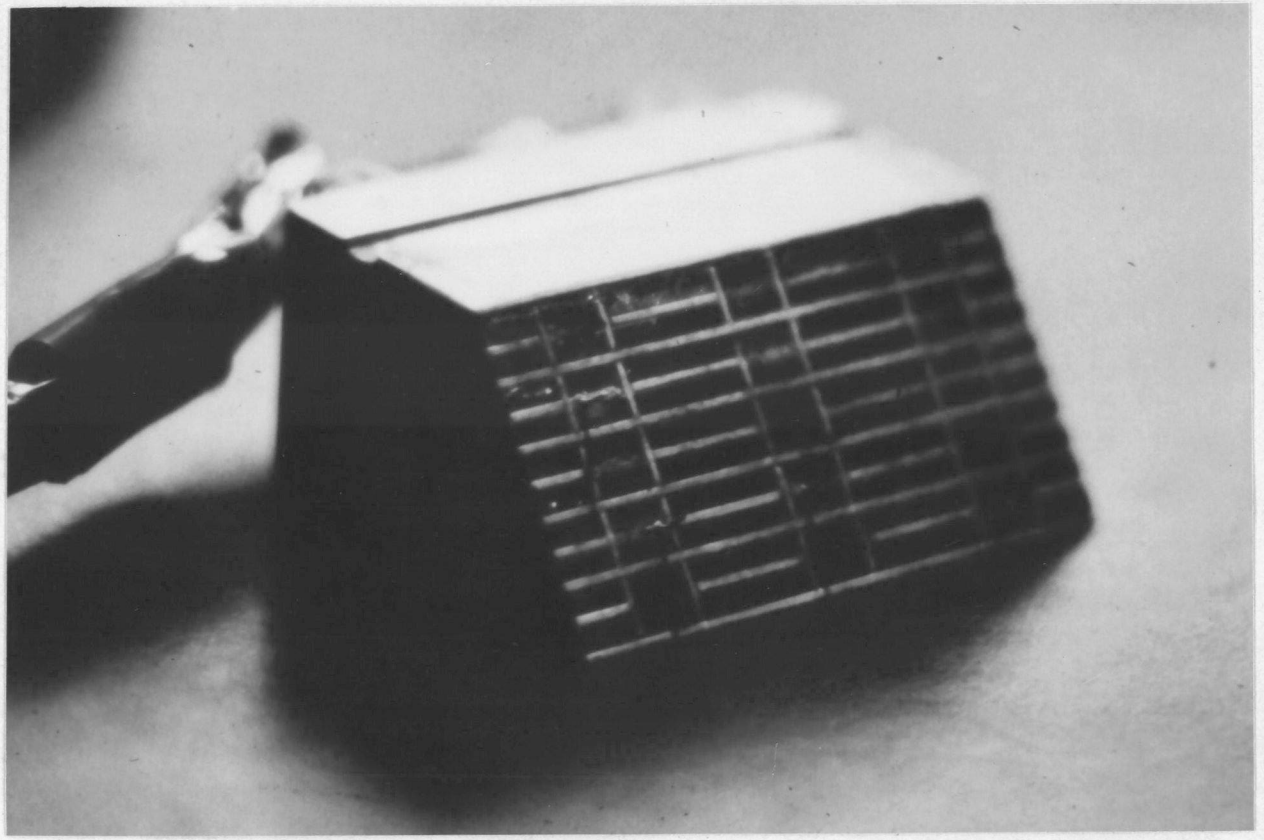


Figure 3. The segmented electrode after the installation of the instrumentation.

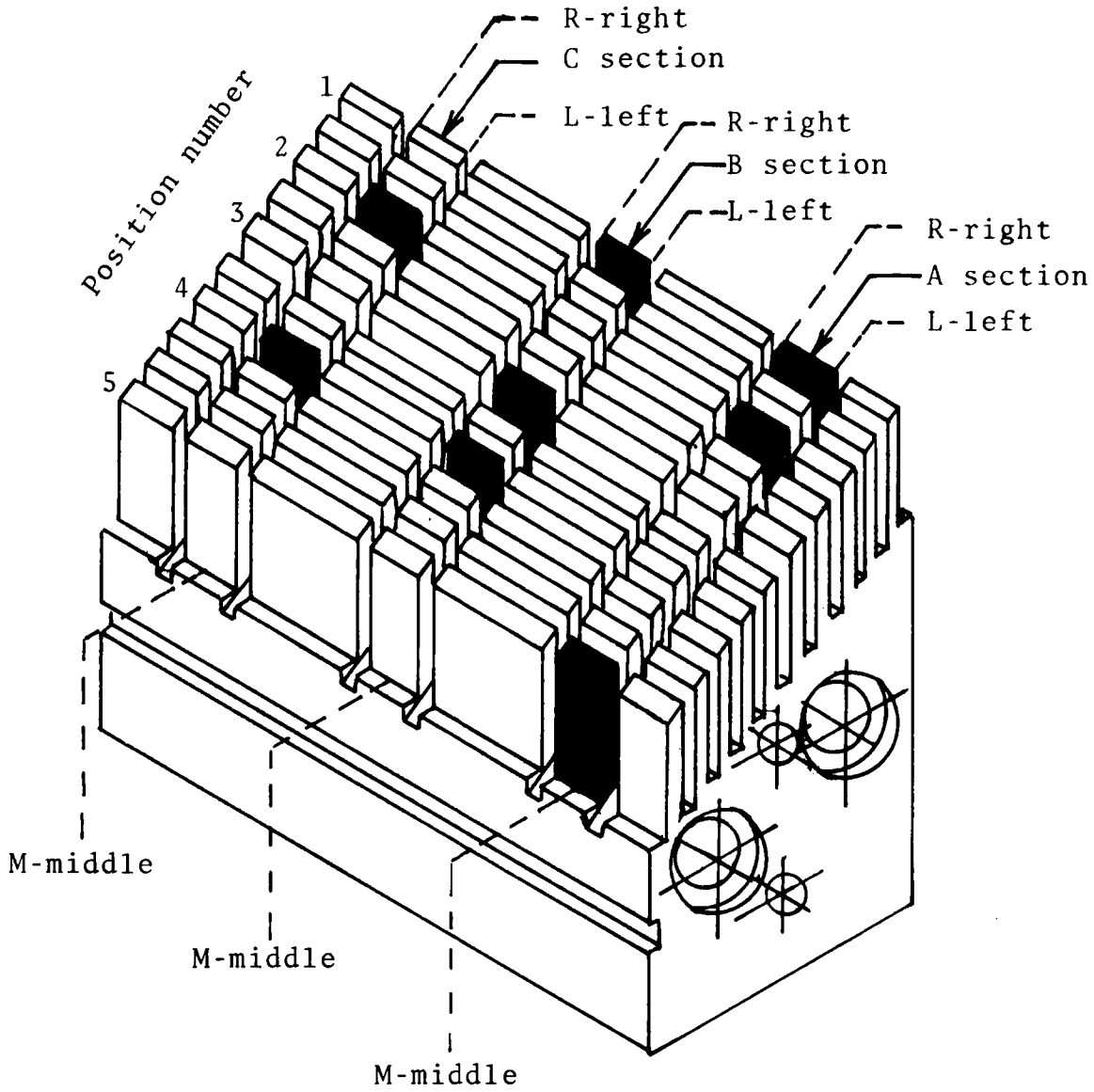
Inconel 625 was chosen as the material which best fulfilled these requirements. The resistivity of Inconel is approximately 80 times that of copper and its thermal conductivity is about one-fourth that of copper. The maximum recommended temperature at which Inconel has reasonable oxidation resistance is 975 C. Other materials considered included stainless steels, Monels, and other Inconels.

## Electrode Segmentation

It was thought that the segmentation should be of the order of mm dimensions. Thus the size of the instrumented segments were designed to be nominally 1.8 mm by 5.5 mm. Experiments conducted on stainless steel segmented with these dimensions indicated that voltage varied by about 10% from one side to the other if current was applied at a point. Similar measurements conducted on the Inconel electrode showed a variation of 25%.

## Electrode Nomenclature

Since there were several kinds of sensing probes which all have specific locations, a special naming system was devised. Referring to Figure 4, instrumentation was placed only in the sections labeled A, B, and C. Within a section, probes were attached only to every other segment. The first segment upstream is labeled number one and the last segment downstream is number five. Left, right, or middle is referred to as L, R, or M, respectively. This




Note:

1. Shaded areas are instrumented segments.

2. M - means in the middle of a section and 1 cm below the surface.

Figure 4. Instrumented segments of the testing electrode.

indicates where the probe lies within a segment. In all cases the probes labeled M are those 1 cm away from the plasma surface. The thermocouples were either called "Op" for open or "Cℓ" for closed. Those designated closed were welded to the Inconel and those designated open were insulated. Inconel 625 wire was used for the positive leg of the current measuring segments and is indicated by I. For example, A1R Pt Cℓ refers to the platinum leg of a thermocouple spot-welded to the Inconel on the right side of segment one in section A. Figure 5 shows the surface facing the plasma and the location of all the surface instrumentation. Table 1 lists the instrumentation according to its Vidar channel.

Electrode Instrumentation

Instrumentation on the electrode was of three types: probes protruded into the plasma; voltage probes were spot-welded to the Inconel near the electrode surface; and thermocouples were placed in three positions. Six thermocouples are near the surface and welded to the Inconel; six are near the surface and insulated from the Inconel; and ten are 1 cm away from the plasma surface.

Four, 20-mil platinum wire voltage probes are insulated from the Inconel and serve as floating Langmuir probes. These are connected to operational amplifier circuits which serve as attenuators and impedance matches between the probes and Vidar data system voltmeter. The

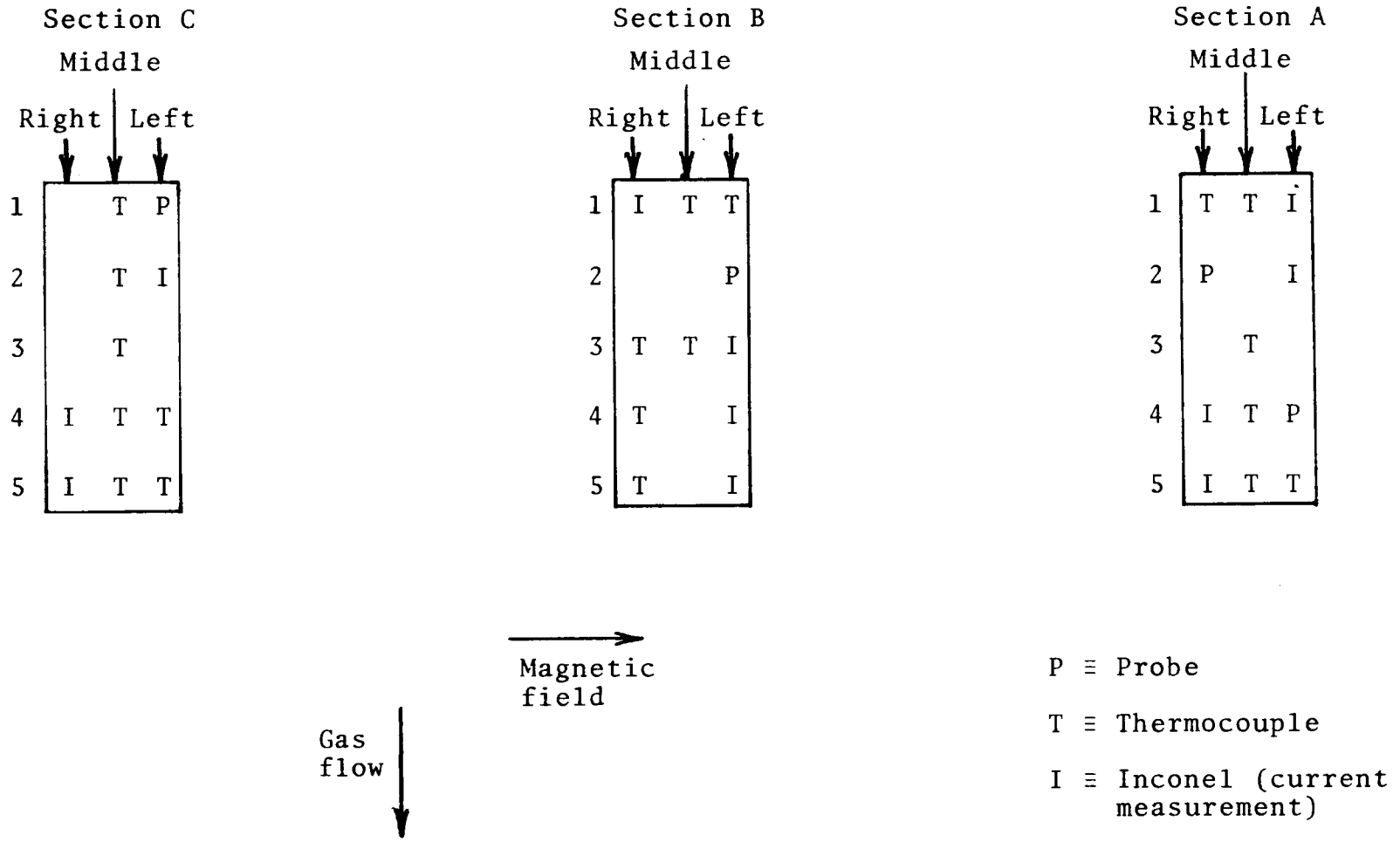



Figure 5. Location of all instrumentation as viewed at the plasma-Inconel interface.

Table 1

Vidar Channel Identification

| Channel | Failed on Run No. | Nomenclature | Channel | Failed on Run No. | Nomenclature |
|---|---|---|---|---|---|
| 0 | 1482 | A4L(probe) | 25 | 1483 | C5L Cℓ |
| 1 | 1482 | A2R(probe) | 26 | 1491 | Thermistor |
| 2 | 1482 | B2L(probe) | 27 | NF[a] | B3L(current) |
| 3 | 1482 | C1L(probe) | 28 | 1484 | C4L(current) |
| 4 | NF | Battery (thermistor) | 29 | 1484 | C4L Cℓ |
| 5 | 1491 | Thermistor (37.6 ohms) | 30 | 1486 | C4L Op |
| 6 | 1483 | A5M | 31 | NF | B3L(current) |
| 7 | 1483 | A4M | 32 | NF | A1L(current) |
| 8 | 1483 | A1M | 33 | 1483 | A1R Cℓ |
| 9 | 1483 | A3M | 34 | 1483 | A1R Op |
| 10 | NF | B1M | 35 | NF | B3L(current) |
| 11 | 1483 | B3M | 36 | 1484 | B4L(current) |
| 12 | NF | C4M | 37 | NF | B4R Op |
| 13 | NF | C2M | 38 | NF | B3L(current) |
| 14 | 1483 | C1M | 39 | 1483 | B5L(current) |
| 15 | 1483 | C3M | 40 | 1483 | B5R Op |
| 16 | NF | B3L(current) | 41 | NF | B3L(current) |
| 17 | 1484 | B3R Cℓ | 42 | 1488 | A5R(current) |
| 18 | NF | B3R Op | 43 | 1483 | A5L Cℓ |
| 19 | NF | B3L(current) | 44 | NF | B3L(current) |
| 20 | NF | B1R(current) | 45 | 1487 | C2L(current) |
| 21 | NF | B1L Cℓ | 46 | NF | A2L(current) |
| 22 | NF | B1L Op | 47 | 1483 | A4R(current) |
| 23 | NF | B3L(current) | 48 | NF | Local Hall Generator Voltage |
| 24 | NF | C5R(current) | | | |

[a]NF: No failure.

relations between the voltage of the probe and the potential of the region is subject to many factors, including the magnetic field, temperature of the probes, and temperature of the surrounding plasma. During the first test, these probes extending about 80 mils above the Inconel were all blown flat because of the 1,000 C temperature and the force of the flow. The data from these probes is unreliable and will not be considered.

The voltage measurements for the current distribution are made using Inconel 625, 17-mil wire spot-welded near (0.5 mm) the surface. This was considered the positive leg and was connected to the positive terminal of the voltmeter. The Pt 10% Rd leg of the thermocouple 1 cm away from the surface was considered the negative leg. Because electrons flow from plus to minus potential, the meter reads negative values when the electrode operates as an anode and positive values as a cathode.

These choices of current probe materials were made so that the thermal emf would be minimized. Even though measurements were taken to determine the thermoelectric power of Inconel at room temperature, these would not suffice for conditions approaching 1,000 C. Although some progress was made toward calculating thermal emf from the thermoelectric power of the metals involved, this method is not considered reliable. As was discovered for some voltage probes during a preliminary test in the range of temperature from 25 C to 130 C, the total thermal emf

actually changed sign. This means that the temperature coefficients of the metals were a significant factor in addition to the normal average thermoelectric power.

The thermocouples are all of the S type (Pt-Pt 10% Rd). Three-mil wire was passed through four-holed, 31-mil O.D. alumina tubing. A rather novel method for forming excellent thermocouple beads on these fine wires was discovered. The wires were simply connected to a power supply capable of 450 volts at 100 milliamps and arced to an electrolyte solution. When the solution was made the anode, better results were obtained than when the solution was the cathode. Perfect spherical beads as large as 1 mm in diameter could be produced, thus making the spot-weld to the Inconel both easy to accomplish and strong. At each current sensing location, a four-holed alumina tube carried two thermocouples near (0.5 mm) the surface. As will be recalled, one was welded to the Inconel and the other was left floating. The Vidar has only 100 db common mode noise rejection. The open thermocouple was designed into the electrode to produce temperature data with reduced fluctuation due to noise. In the experiment, noise did not appear to affect the temperature readings appreciably.

The thermocouples 1 cm from the surface were inserted into holes drilled from the back side of the Inconel. Silver paint was injected into the holes with a syringe to help effect an ohmic contact when the

thermocouples were pushed to the bottom of the hole. Through previous experiments this silver paint was found to maintain a good contact with no visibile discoloration up to 800 C in air.

Electrode Cooling

Because of the many sensing probes placed throughout the segmented electrode, some of them had to necessarily pass through the water cooling passages. These leaked at first but were eventually sealed by a commercial product, "Super Glue" and a similar product, "Eastman 910," the latter being manufactured by Kodak. Static water tests at 100 psi showed no leaks through the passages and only a drop accumulation around the "O" rings. These sealants unfortunately proved ineffective under the conditions of lengthy exposure to water, temperature near 100 C, and 150-psi water pressure. In an emergency effort to stop the leaks after the first test, an uncured rubber, "RTV," manufactured by General Electric, was employed. The coolant passages were completely filled with RTV and then a static pressure in excess of 350 psi was applied to force the rubber around the alumina tubes. After the completion of this process, the RTV was cleaned out of the passages. By this technique the leaks were reduced to a small seepage of one drop per minute at 100 psi. With the electrode in this condition, nine generator tests were run, each of which was two minutes in duration. For the last run the leaks were

again significant, preventing slag from forming on about half of the Inconel surface. This performance was excellent considering the rather unsuitableness of the sealant and the difficult conditions under which the sealing task was performed.

The Inconel electrode cooling passages were aligned with the cooling passages in the copper side wall. Water circulated down one side wall, through the Inconel, and up the other side wall. "O" rings provided a good seal at the copper-Inconel interface. The two water passages in the Inconel were each 0.64 cm (1/4 inch) in diameter and approximately 1.5 cm from the plasma surface.

## Electrode Fabrication

All of the probe wires were connected to 5-mil copper teflon coated extension wires at the back of the electrode. The extension wires were 1.5 m long. These connections were effected by spot welding. When a section had been completed, Sauereisen number 78 electrical cement was used to provide electrical insulation, structural support, and protection for the probes. A thermistor, type UUA-35J3 from Omega Engineering, Inc., was cemented into the center section to provide the reference temperature for the probe thermocouples. Finally, the extension wires were wrapped with aluminum foil and taped with electrical tape for shielding, protection, and insulation.

With the probes in place, the machined grooves were filled with slabs of ADS 99.5% alumina, manufactured by Coors Porcelain, as a semiconductor substrate material. Each piece needed to be cut for a specific location since the machining of the slots had not been uniform in length or depth. By this method of measure and cut, tolerances of between 1 and 2 mils were obtainable. The thickness of the slabs matched the width of the cuts so closely that binding material was unnecessary. Fabrication was greatly simplified because of this extraordinary fit.

On the current sensing segments, Sauereisen was used to fill between the two, 31-mil alumina tubes. Recall that on each segment, one tube was for the current sensor and one tube for the temperature. This material is much less resistant to slag penetration and erosion than high purity alumina cements. Unfortunately, these pure cements need to be fired at 1,000 C for a hard finish. The teflon coating and sealant prevented any such high temperature firing.

To finish the irregularities to a tolerance of 1 or 2 mils, a Futura Starflight dentist drill powered with nitrogen gas was used. The alumina slabs were cut using a Buehler Ltm. Isomet saw with a low density diamond wheel blade.

## Vidar System Instrumentation

The Vidar digital acquisition system is a multi-channel system that scans, measures, and records the input voltage signal on each channel. The voltage signals are read by a model 502 B integrating microvoltmeter. The readout is by means of printed paper tape. The scan may be run in a continuous mode as it was in this experiment. The printer is the slowest component of the system, having a data print rate of approximately 20 cycles per second. Since the number of channels utilized was 69, the total scan time was about three seconds. One complete scan was called a data set in this work.

The system also has a clock that provides the time to the nearest second to the printer. Since the scan rate for each data set may be assumed to be nearly constant and since the repetition rate of the printer is known, time during a data set may be obtained within 40 milliseconds.

## Grounding and Noise Effects

Common mode noise as well as normal mode voltage can cause a meter to read voltage when it should not. From Nicholson [5] the voltage fluctuation at electrode numbers 22 and 23 is about 30 volts peak to peak. The maximum normal mode voltage that the Vidar can accommodate without damage is 200 volts. It is specified as having 150 db normal mode rejection at DC. However, measurements conducted on the system indicated the DC rejection was

closer to 130 db. For example, when 200 VDC was applied to the positive terminal, -58 ± 2 microvolts was recorded by the meter. For AC signals, the meter counts and obtains an upper and lower bound for a given frequency and amplitude of noise. When DC normal mode voltage was applied in addition to AC common mode, the upper and lower bounds were shifted in the negative direction. If the DC voltage is known, the signal can be corrected for normal mode effects.

The AC common mode rejection, as specified for the Vidar, is 120 db at all frequencies. Checks on the system indicated at best only 100 db, however. Below 16 Hz the CMR rejection depends chiefly on guarding and shielding. About 10% of the rejection near this frequency is due to the integration method of voltage determination. At frequencies of 600 KHz or more the roles of integration and guarding are reversed since guarding now provides only 10% of the rejection. Since noise frequencies in the channel are almost all below 20 KHz, shielding becomes very important. Consequently, shields are utilized all the way to the Inconel block in the generator. Figure 6 shows the connections of the shields from the Vidar to the terminal box and also to the foil around the copper extension wires.

The input impedance of the Vidar is greater than 10 megaohms on the 10-millivolt scale. Therefore, the meter will draw 20 microamps when the input potential is 200 volts on the generator.

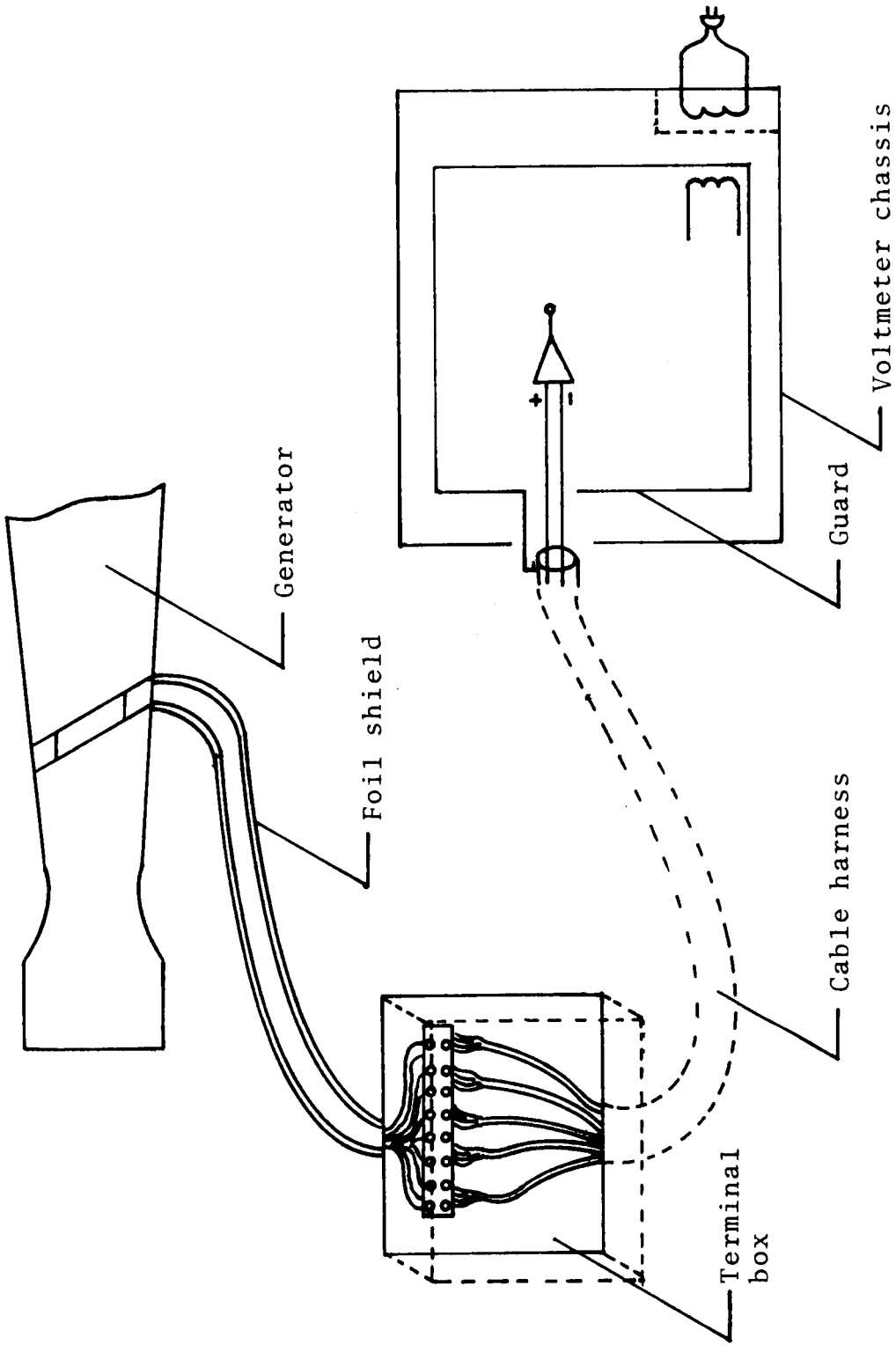
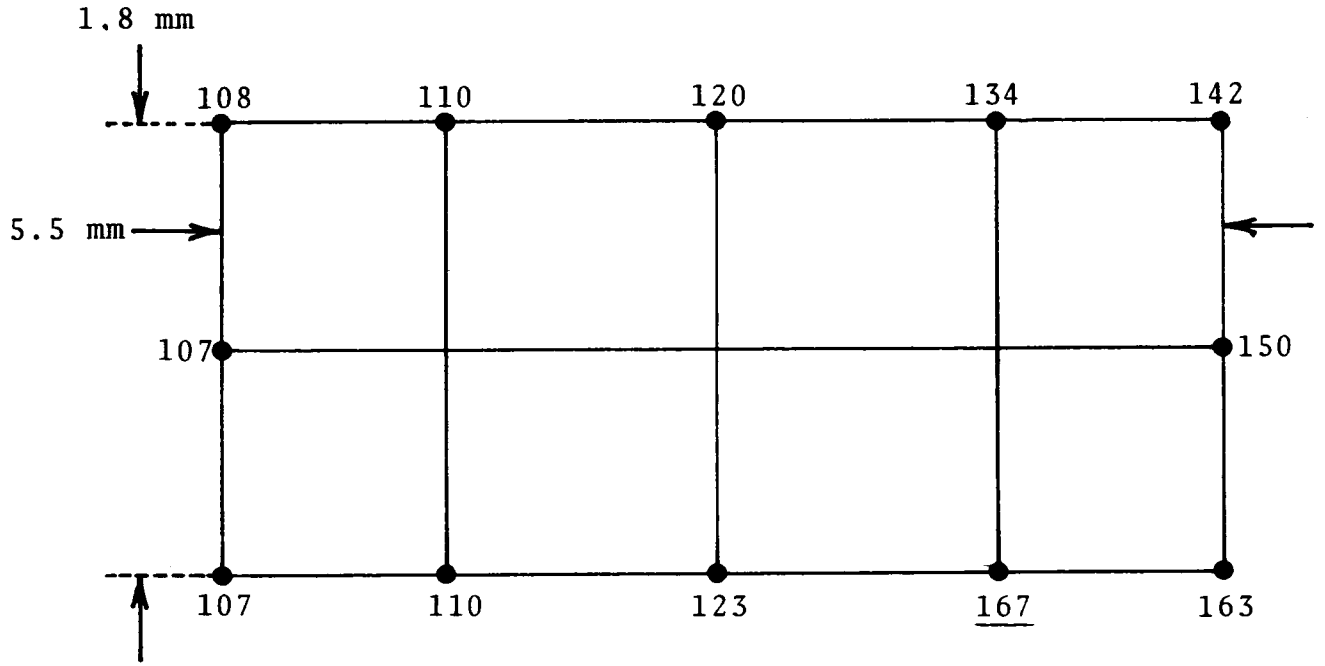



Figure 6. Shielding of instrumentation wires.

Calibration of the Electrode

It was realized that the resistance in the Inconel segments could not be determined easily from the resistivity, the dimensions of the segments, and positions of the probes. Therefore, experiments were undertaken to measure the voltage drop when 100 milliamps of current was applied to each segment. Voltage drop varied among segments and also according to the position of the current application relative to the sensing probe. Current was applied using a sharp-pointed probe. The maximum voltage was always observed when the current was applied directly over the sensing probe, as would be expected. The variation in observed voltage was not insignificant as the current probe was moved from side to side and from end to end on each segment. Figure 7 represents the variation on a typical segment, A1. The underscored value represents the position directly over the probe. All readings are in microvolts. Cross talk between segments was found to be not more than 5 or 10 microvolts. That is, when 100 milliamps was flowing in one segment, voltage was observed on an adjacent segment.

A simple average of voltages from not less than ten positions for each segment was taken as the calibrated signal for an arbitrarily applied current of 100 milliamps. Table 2 lists the arrived at figures for each segment. Table 3 lists the dimensions of each segment at the plasma-Inconel interface.




Note:

1. All readings are in microvolts.
2. Underscore is the position of the voltage probe.
3. Data is for segment A1.
4. The current applied is 100 milliamps.

Figure 7. Positions of nonequipotential on the electrode surface with current applied at the center point.

Table 2

Calibration for each Segment at 100 Milliamps

| Segment | Av. Voltage (microvolts) | Area ($cm^2$) |
|---|---|---|
| A1 | 128 | 0.116 |
| A2 | 153 | 0.098 |
| A4 | 152 | 0.098 |
| A5 | 124 | 0.126 |
| B1 | 140 | 0.119 |
| B3 | 144 | 0.105 |
| B4 | 150 | 0.098 |
| B5 | 121 | 0.126 |
| C2 | 152 | 0.095 |
| C4 | 143 | 0.095 |
| C5 | 120 | 0.126 |

Table 3

Dimensions of each Segment at the Plasma Surface

| Segment | Length (cm) | Width (cm) |
|---|---|---|
| A1 | 0.549 | 0.211 |
| A2 | 0.551 | 0.178 |
| A3 | 0.551 | 0.191 |
| A4 | 0.551 | 0.179 |
| A5 | 0.551 | 0.229 |
| B1 | 0.551 | 0.216 |
| B2 | 0.546 | 0.165 |
| B3 | 0.551 | 0.191 |
| B4 | 0.551 | 0.179 |
| B5 | 0.551 | 0.229 |
| C1 | 0.551 | 0.216 |
| C2 | 0.551 | 0.173 |
| C3 | 0.551 | 0.183 |
| C4 | 0.551 | 0.173 |
| C5 | 0.551 | 0.229 |

## Thermal Effect on Resistivity

The temperature effect in the range from 25 C to 1,000 C on the resistivity of Inconel is found to be about 6%. Data was taken from the Huntington alloy source book [11]. The calibrated values in Table 2 are adjusted to include this temperature dependence.

## Run Procedure

The total number of ten runs may be divided into two sets, the initial test and the remaining nine. The first test had a multiple load, as shown in Figure 8. The run time was eleven minutes. The first minute was with kerosene to preheat the generator. Following were four intervals of time, each used to make a specific study. Immediately after the kerosene burn, followed three minutes of coal/seed burn using full magnet power for the first current distribution study. The magnet was then turned off for two minutes to obtain thermal data only. Four minutes followed for the second current distribution study with the magnet back on. The longer time was to assure good slag coverage. Finally, one minute of run time was made with the first few electrodes shorted in order that the effect of a change in voltage could be recorded.

The second set of runs had both a simpler and shorter procedure. Preheat was again used, but only for 30 seconds. The run time on coal which followed was

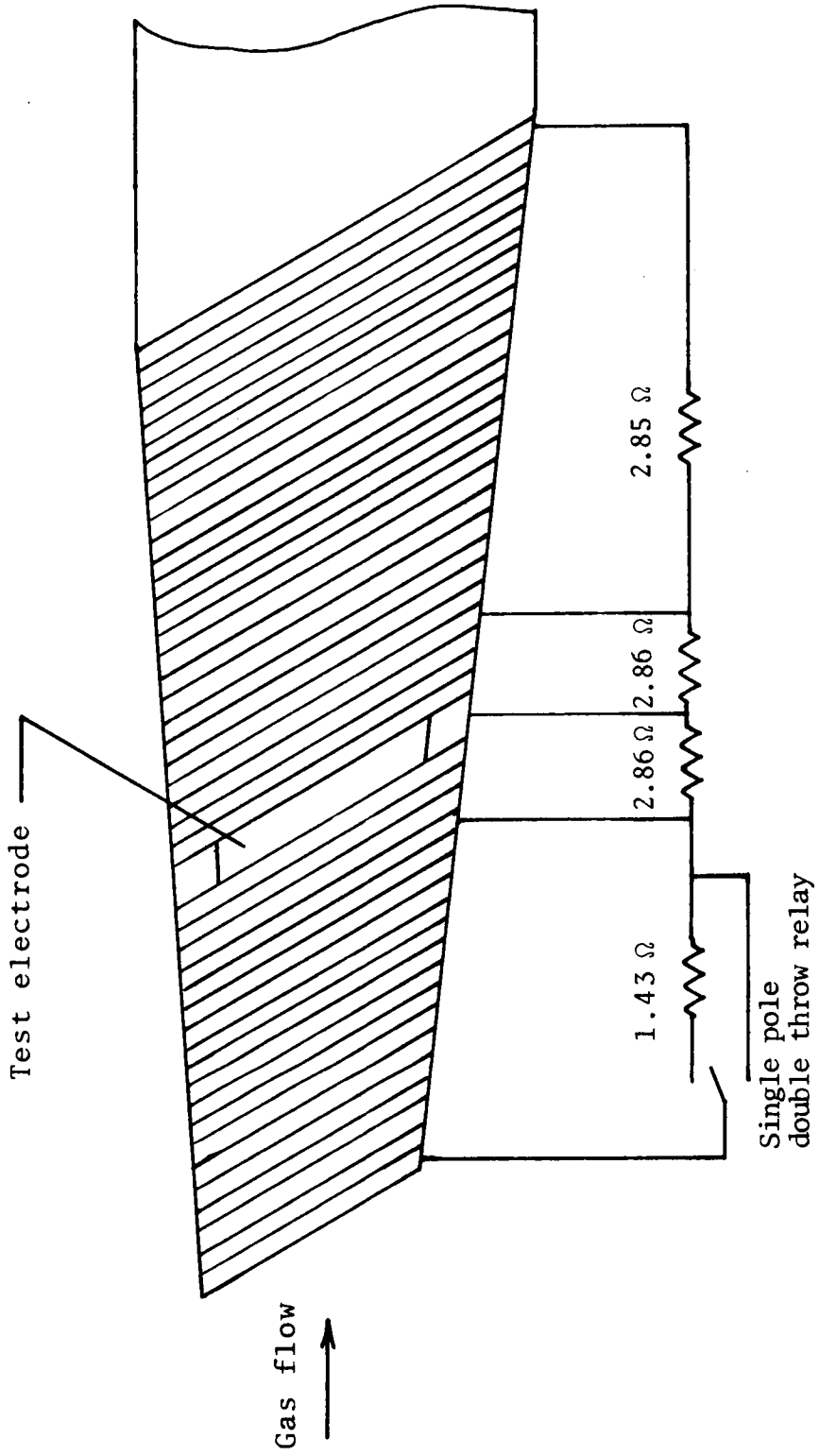



Figure 8. Generator multiload configuration.

90 seconds. This period was divided into three equal sub-periods to accommodate the changes in the load. The two-terminal load configuration was used with values of 10 ohms, 6 ohms, and zero ohm. This was also the chronological sequence as the load was changed. (See Figure 9.)

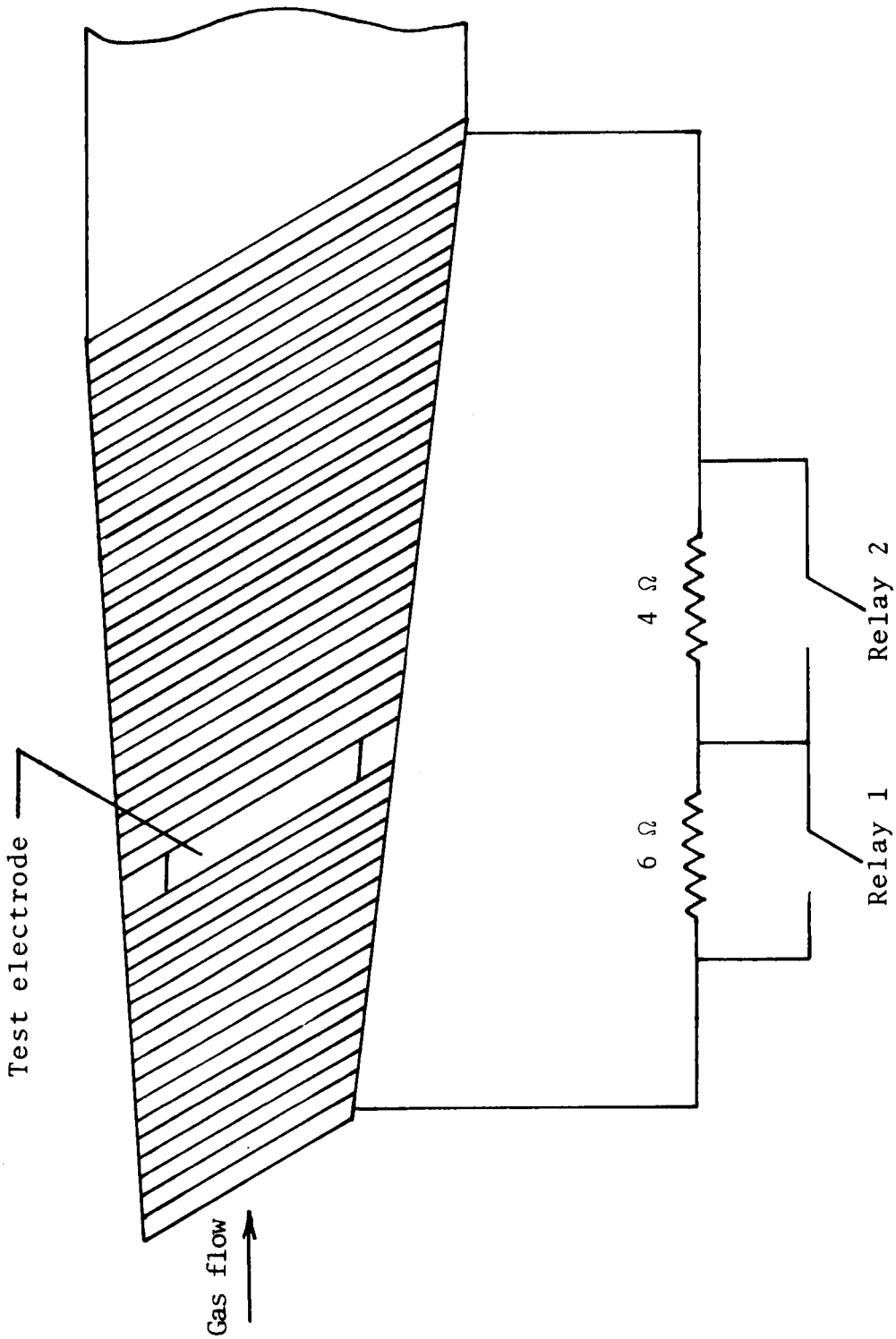



Figure 9. Two-terminal load configuration with relays for load switching.

# CHAPTER III

## DISCUSSION OF DATA

### Synopsis of the Tests

As has been already mentioned, the experiment consisted of ten runs on the DCW generator. Problems arose both with the segmented electrode and with the generator which necessitated the large number of runs. The best possible power output on the generator was desired. Because of the deteriorating condition of the insulators between the electrodes, the maximum power achieved was low, approximately 39 KW. Following is a short description of each test run.

1. Number 1482 gave good power, but because of an oscillograph malfunction, no strip chart current-voltage data was recorded. Both the segmented electrode and the panel meters showed current. This test developed water leaks on the segmented electrode about 18 seconds into the coal-fueled period.

2. Numbers 1483 through 1486 are runs where the water leaks had been stopped, but where the generator was shorted in several places. Generator cooling lines were shorted to the magnet in one case; the diffuser made contact with a bolt in part of the undercarriage support of the generator for another; and finally, arcs to the magnet pole face had developed through torn mylar insulation. This

last difficulty required the disassembly of the generator. At this point gas leaks were also discovered in the vicinity of electrode number 22. Good slag was found on the Inconel.

3. Number 1487 represents the best power run with about 39 KW output. See Figure 10 for the load line curves. Photographs were taken with a boroscope of the slag covered Inconel.

4. Number 1488 is a run made with the magnetic field reversed. The power is poor, as would be expected.

5. Numbers 1489 and 1490 were runs that had shorts in the conductivity section downstream of the diffuser.

6. Number 1491 produced about 38 KW of power, but this was discovered later to represent a peak value. The load line shows that power deteriorated during the last half of the run. The segmented electrode was again beginning to leak water. As a result, slag covered only about one-half of the electrode.

Discussion of Data on Run Number 1482

Number 1482 was the multiload test. The load was distributed such that the Hall field would be as small as possible in the vicinity of the segmented electrode. Total load on the generator was 10 ohms. As may be seen from Figure 8, page 33, current was allowed to leave the generator through the test electrode. It is believed that the current density and current concentration became higher as a result. As will be shown from later tests, current

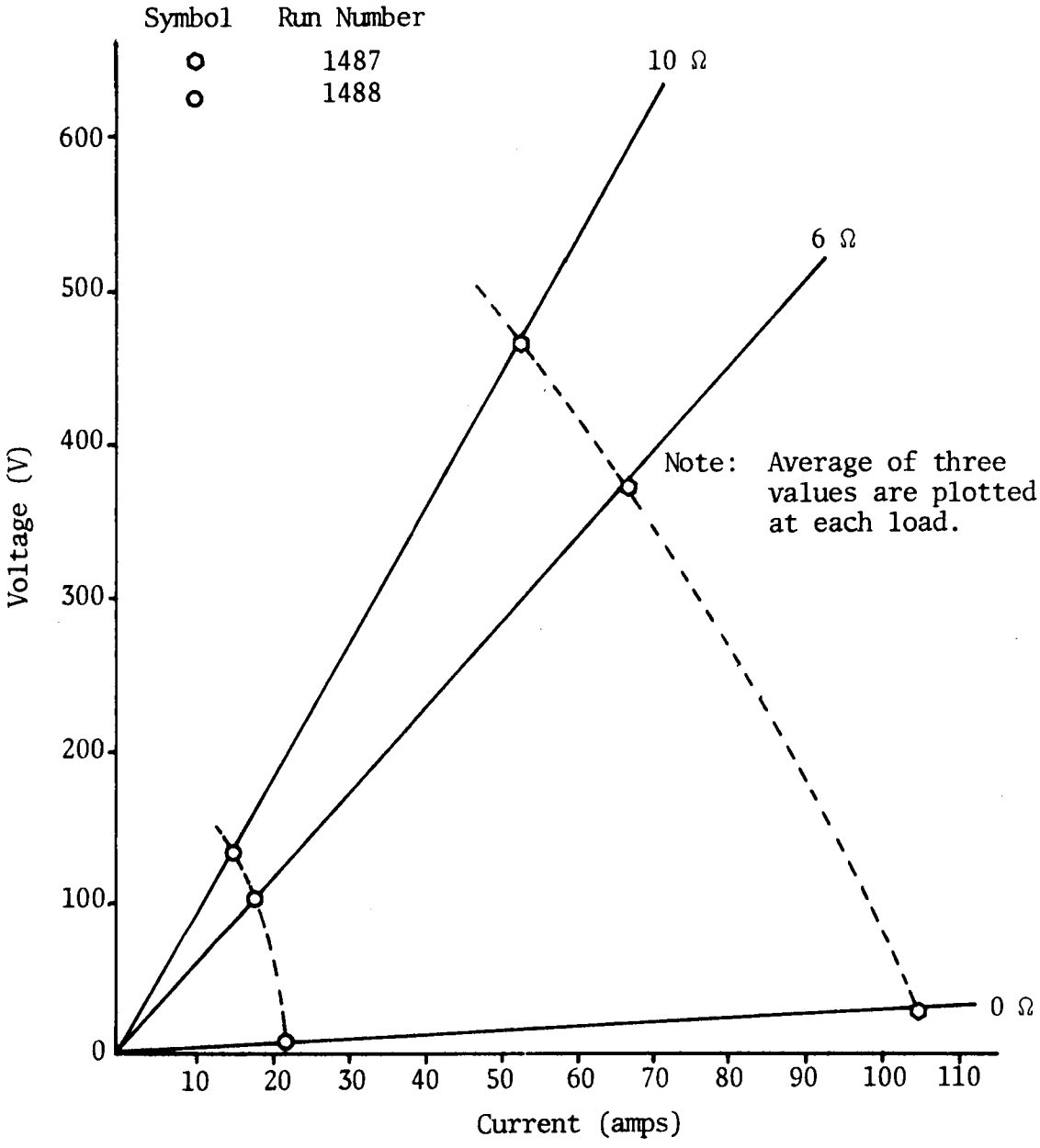



Figure 10. Load line curves for tests that produced measurable power.

concentration on the test electrode is not directly indicated by the data when the generator is in two-terminal operation.

Because of water leaks that developed, the surface temperature fell to the temperature of the back surface. That is, the thermocouples were observed to produce zero voltage. After coal had been burning approximately 18 seconds, the segmented electrode was thoroughly cooled, as shown in Figures 11 and 12.

It is seen in Figure 11 that the surface temperature dropped from 980 C to less than 100 C. Segment C4 was not conducting greatly until data set 34, about 42 seconds after coal on, as shown in Figure 13. Upon extensive conduction, however, the temperature on the surface of C4 went up to 1,040 C. See Figure 11.

The plot for C4M in Figure 14 is the uncorrected temperature and shows a peak value of approximately 970 C. Other middle thermocouples are relatively cool. The high value of temperature for C4M is attributed to the high current being conducted on C4. The C4M temperature and current remained relatively constant during the remainder of the run until the magnetic field was turned off.

Therefore, temperature increased dramatically at the surface where current concentrated. This occurred in spite of extensive cooling by leaking water.

The current was concentrated downstream and near the side wall. As much as 40 amps was observed to flow through

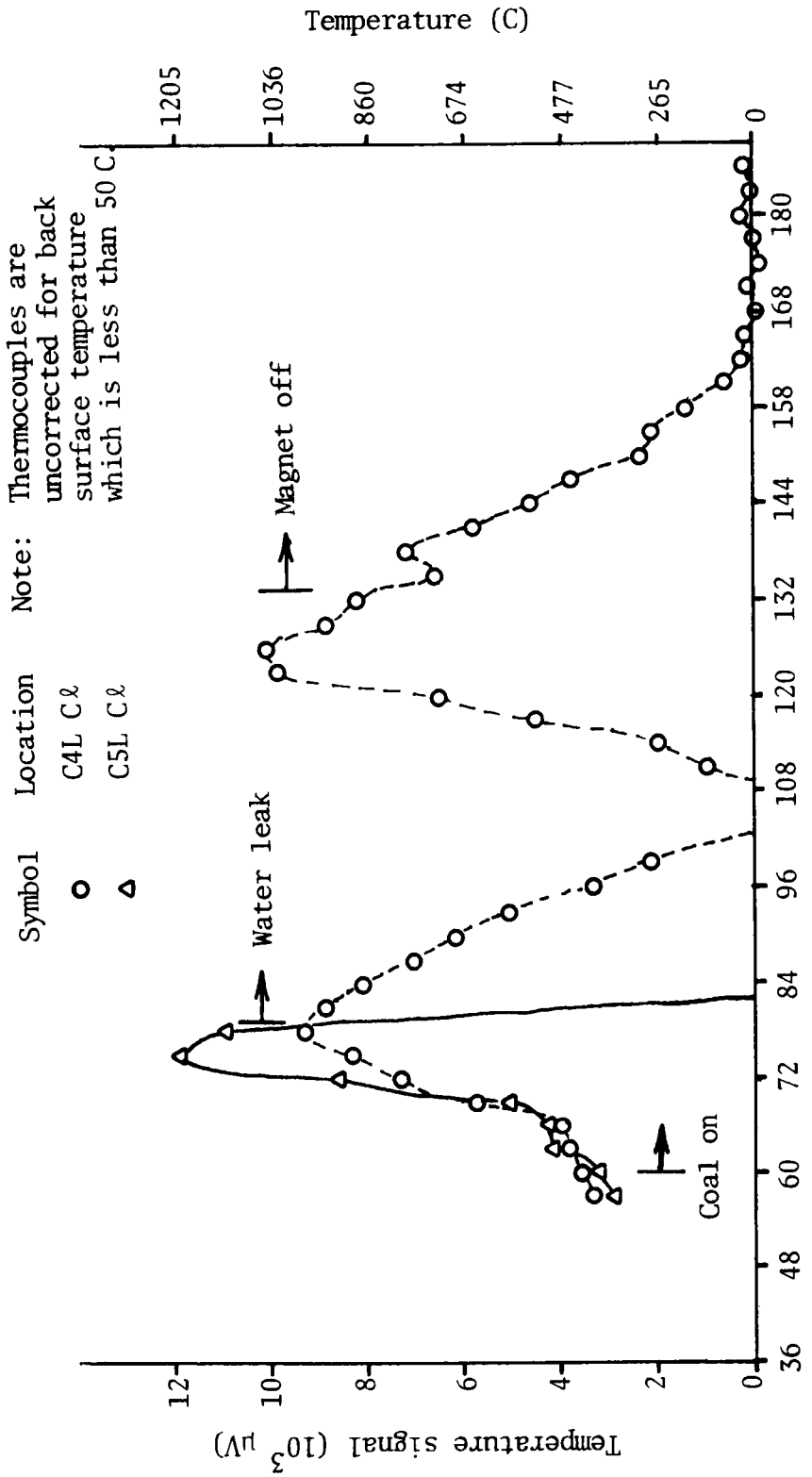



Figure 11. Temperature versus time plot of surface type S thermocouples on run number 1482.

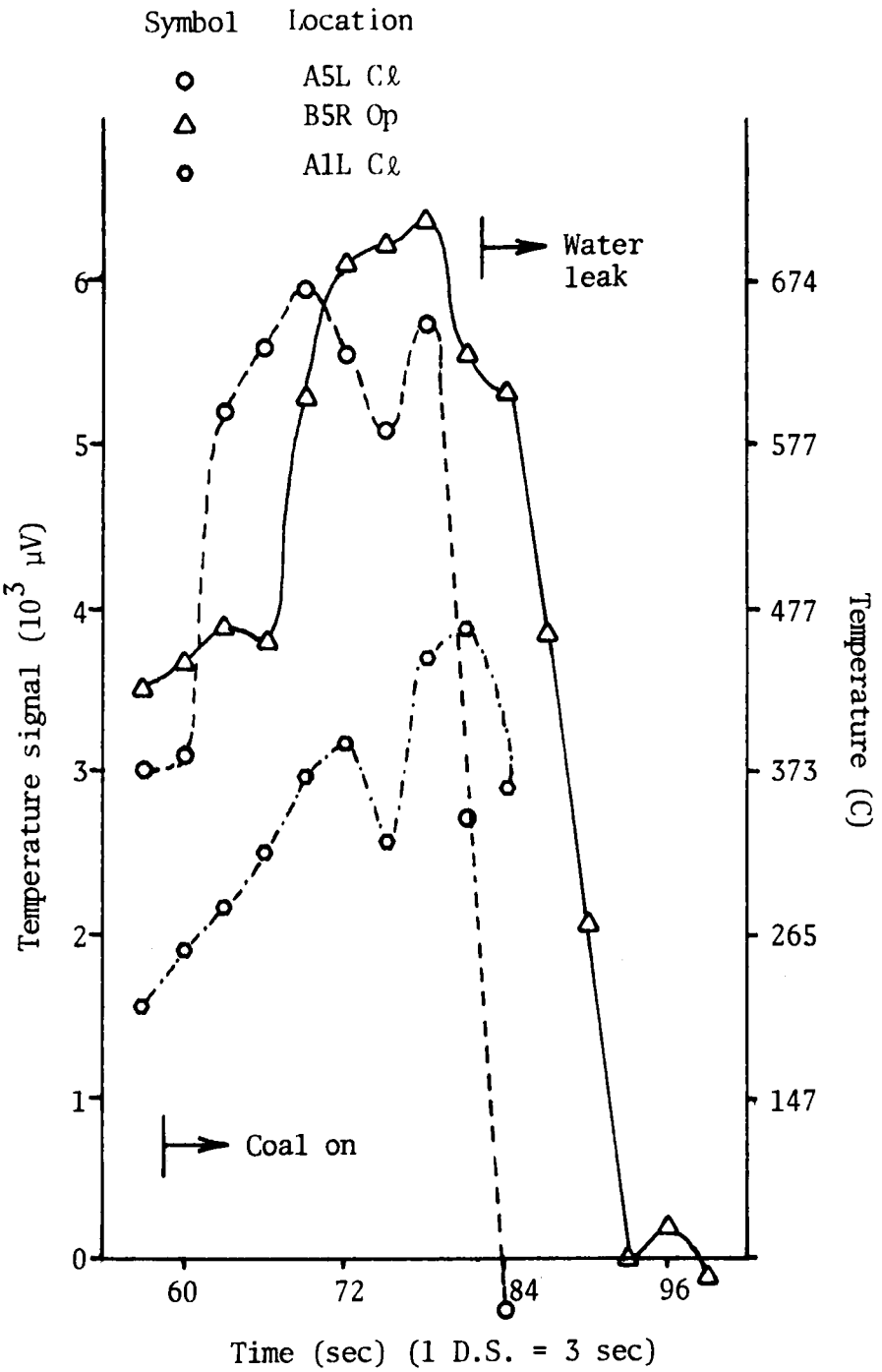



Figure 12. Temperature history of segments for run number 1482.

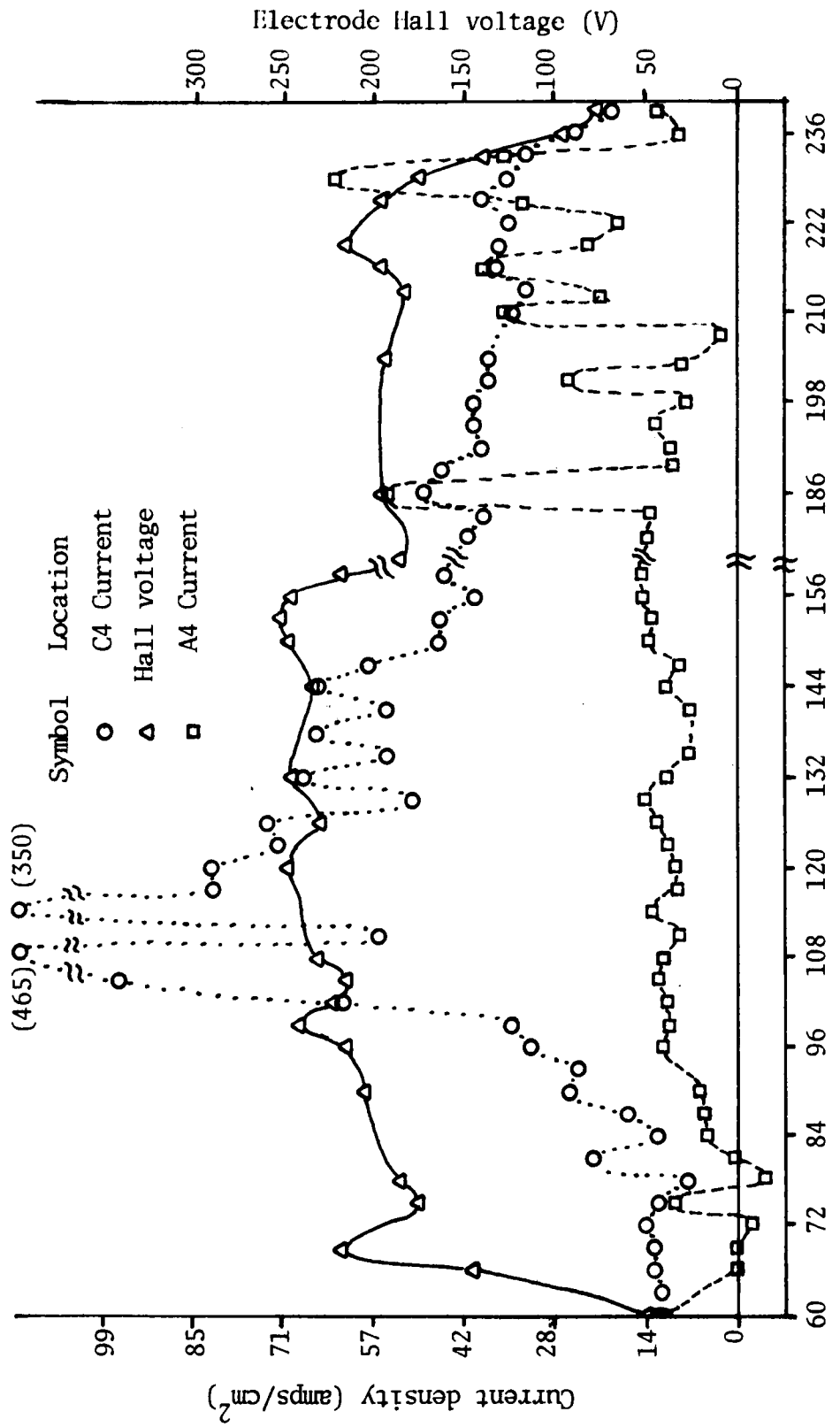



Figure 13. Current density and Hall voltage on C4 and A4 segments plotted versus time for run number 1482.

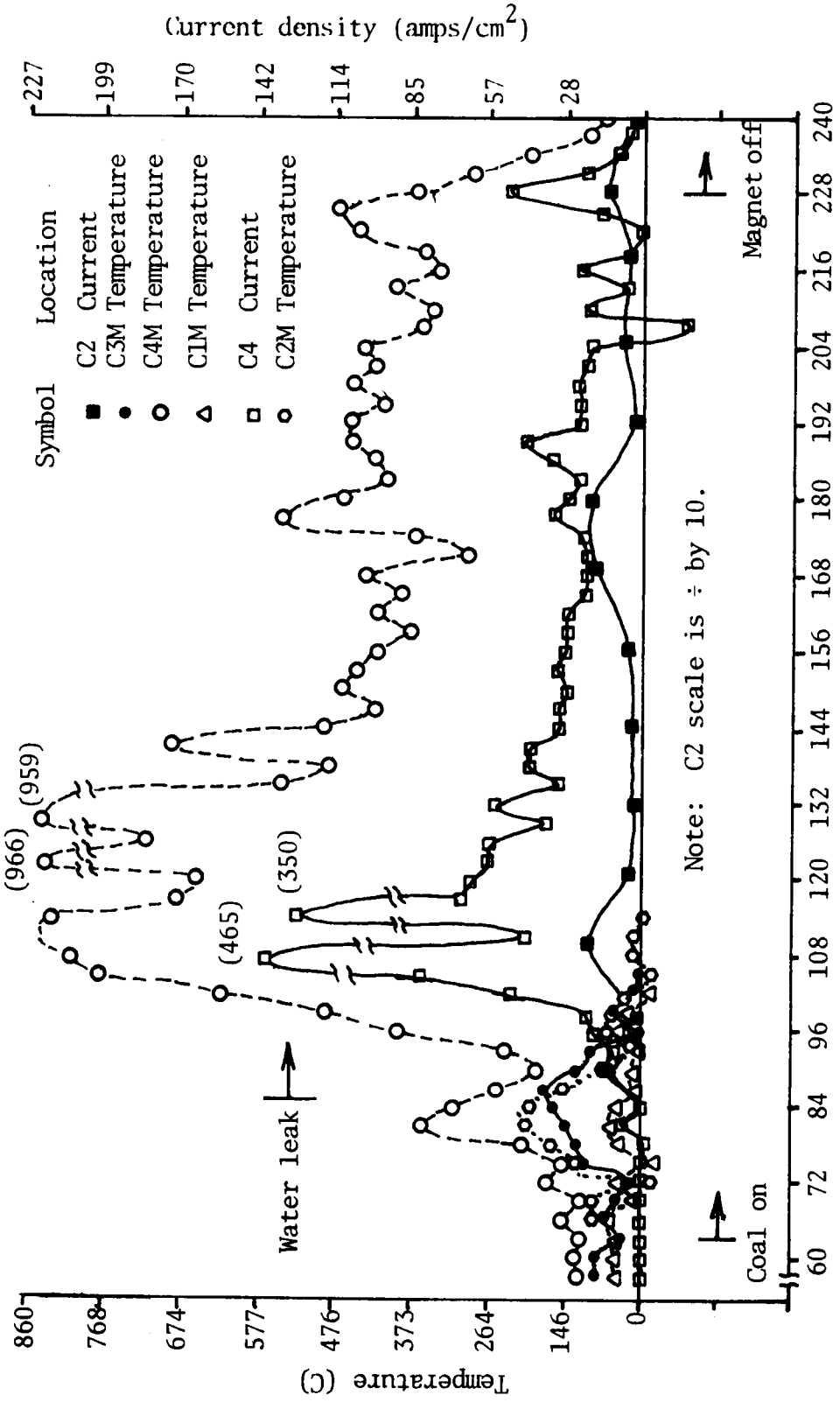



Figure 14. Temperature and current density history of segments on run number 1482.

a single segment. During calibration, cross talk was observed to be between 5 and 10%. Figure 14 indicates that C4 carried a large current, but C2, little. For example, if C4 is carrying 71 amps/$cm^2$, then C2 should read about 7.1 amps/$cm^2$. The data indicates that 7.1 amps/$cm^2$ was not exceeded. Since the C2 signal is generally smaller than that expected from cross talk, electrons must be flowing out of this segment.

During the first 27 seconds after coal on, the electrode was operating chiefly as a cathode since the polarity of the voltage signal is taken as an indication of the direction of electron flow. See Figure 15 for this effect where cathode behavior is plotted in the negative direction. One sees from Figure 13, page 42, that the voltage is rising to nearly 200 volts during this period. The voltage of the test electrode is taken with respect to ground potential.

Figure 16 is similar to Figure 13 and shows that current is still being concentrated on C4, but is slightly reduced in magnitude. Further, it can be seen that both voltage and current are less erratic when the generator has been running for a longer time. Two minutes of test time with the magnet off separate the periods shown in Figures 13 and 16.

Since the current concentrated to a high degree in this test, it does not seem inconceivable that essentially all the current on the Inconel flowed through a single

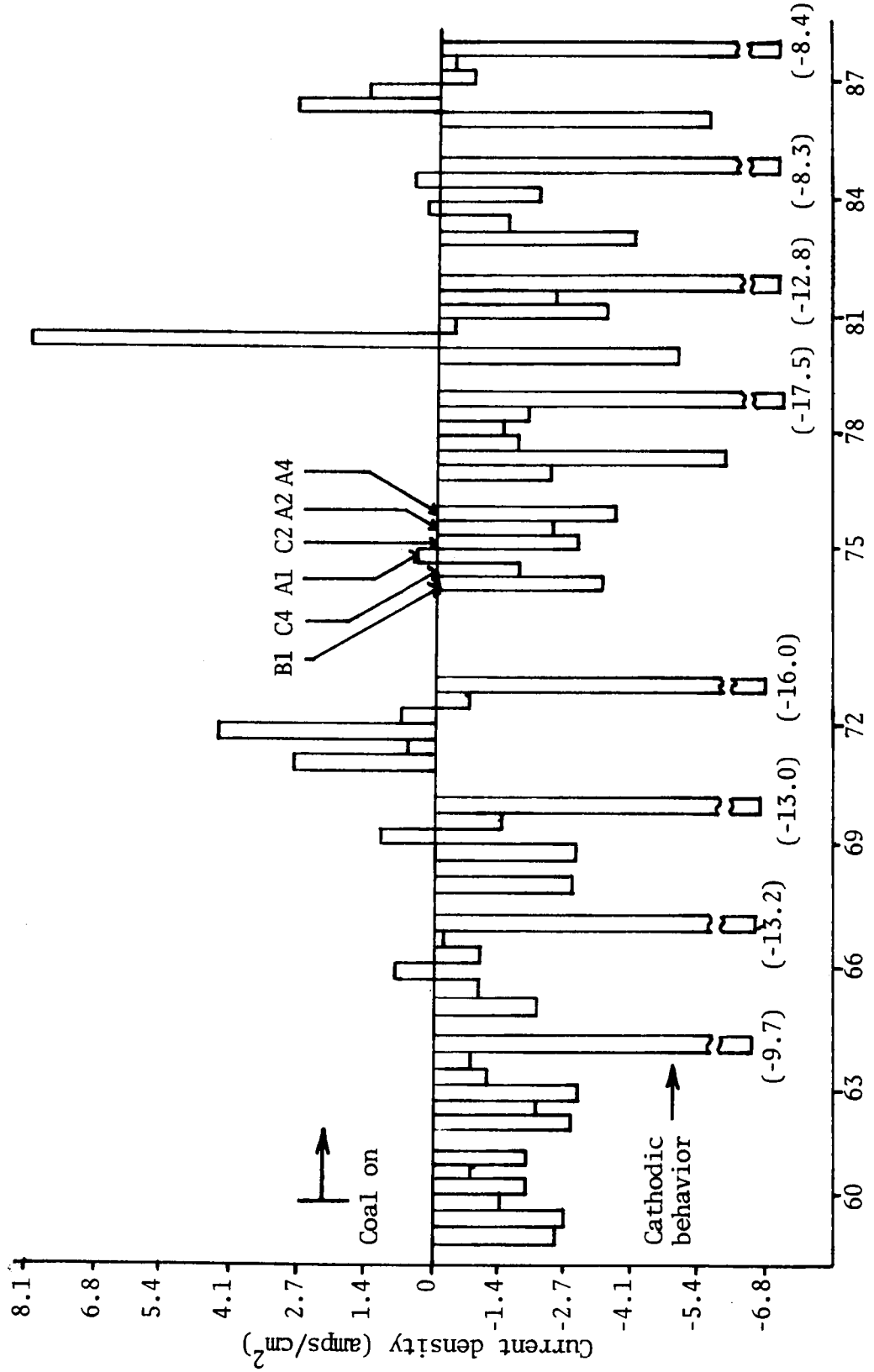



Figure 15. Histogram of initial cathodic behavior on the collecting electrode for run number 1482.

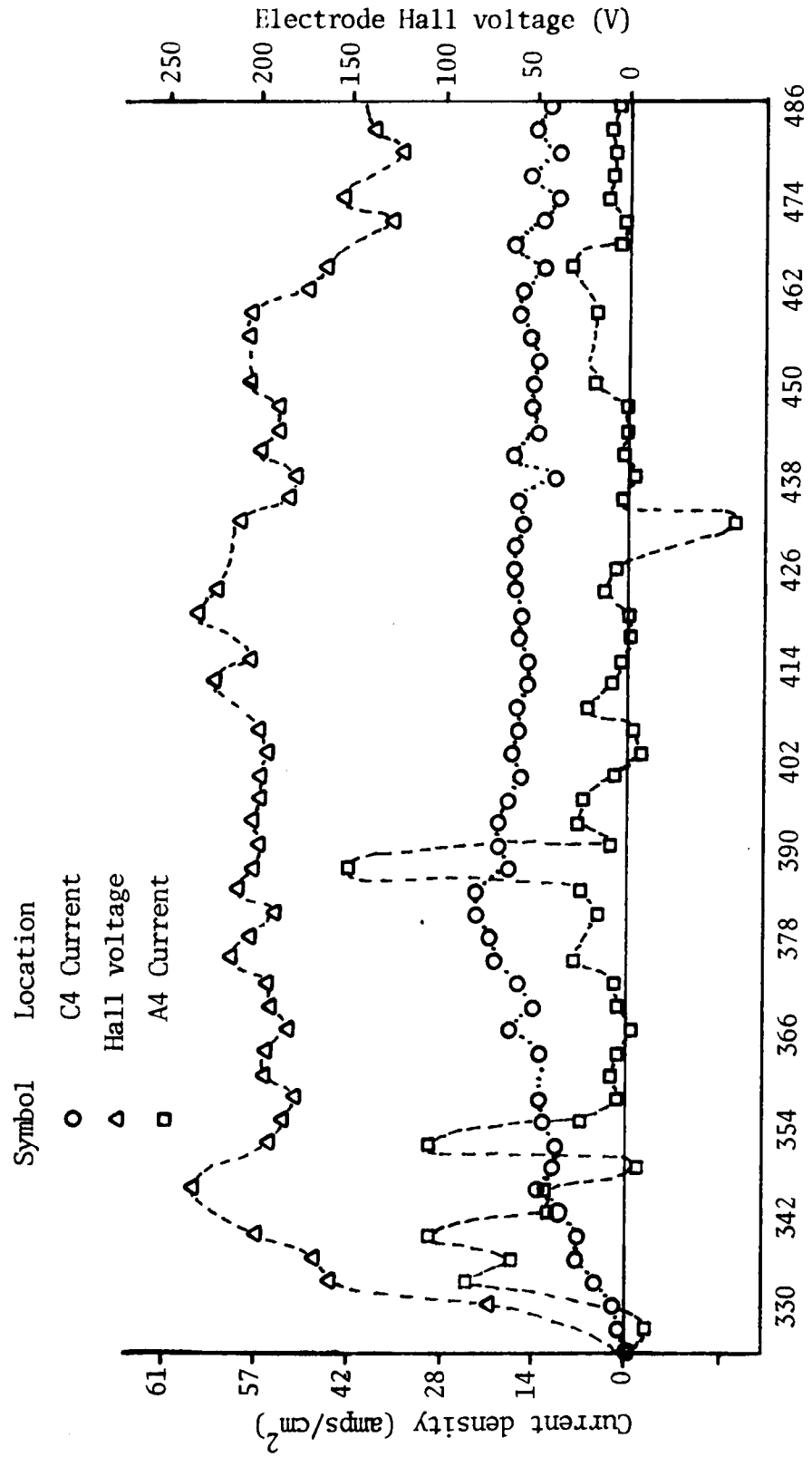



Figure 16. Current density and Hall voltage for run number 1482 plotted versus time when magnetic field is turned back on.

segment, that segment being C4. The total area of the Inconel is very nearly 13 $cm^2$. The current density is then about 3 amps/$cm^2$ for the peak value, a figure that is very reasonable.

After the first run, the electrode was taken out of the channel and observed to have no obvious erosion. The electrode, it will be recalled, was very cool during most of this run. Because of the extremely cold wall and the spraying water, no slag whatever adhered to the Inconel during this run.

Discussion of Data on Run Number 1483

Photographs were obtained after this run by taking the injector off and thrusting a boroscope down the channel through the combustor. Using the lens system of the boroscope and a hood over a 35-mm camera with the objective removed, reasonable slides of the excellent slag coating over the Inconel were obtained. The slag coating appeared to be very evenly distributed with a thickness of roughly 1 mm. The copper had not sufficient time to obtain a coating. Also observed were several small holes of about 1-mm diameter randomly distributed in the slag over the electrode.

Since there was good slag coverage, it was known that the water leaks had been stopped. In the course of eliminating the leaks, the A section probe wires were torn

off. It was possible to repair the current probes, but the thermocouples were hopelessly mangled.

The load, it will be recalled, was of the two-terminal type for all runs after the first one. The total time for each run was two minutes, after which shut-down was immediate.

The first observation concerning the current is that after coal on, the current rises to a peak in about 12 seconds and then descends in about the same time to one-half the peak value. For the remainder of the run, oscillations dominate and the current steadily decreases, as seen in Figure 17. The decrease in the magnitude is believed due to the decreasing temperature of incoming oxygen. A graph of events for run number 1483 is shown in Figure 18. Also shown is the mean, standard deviation, and deviation in the mean for each data set. The mean appears to be oscillating with a period of from 12 to 18 seconds. A comparison with oscillograph data of total current and total voltage shows oscillation of the same period.

Figure 19 shows the time average current as the load is changed. The bars indicate the deviation in the mean and show that the smaller current has less fluctuation. It should be noted that during this run the channel was shorted to ground in three places. As a result the current does not reflect the loads as it should.

The thermocouples indicated that the temperature was behaving as might be expected, reiterating that the water

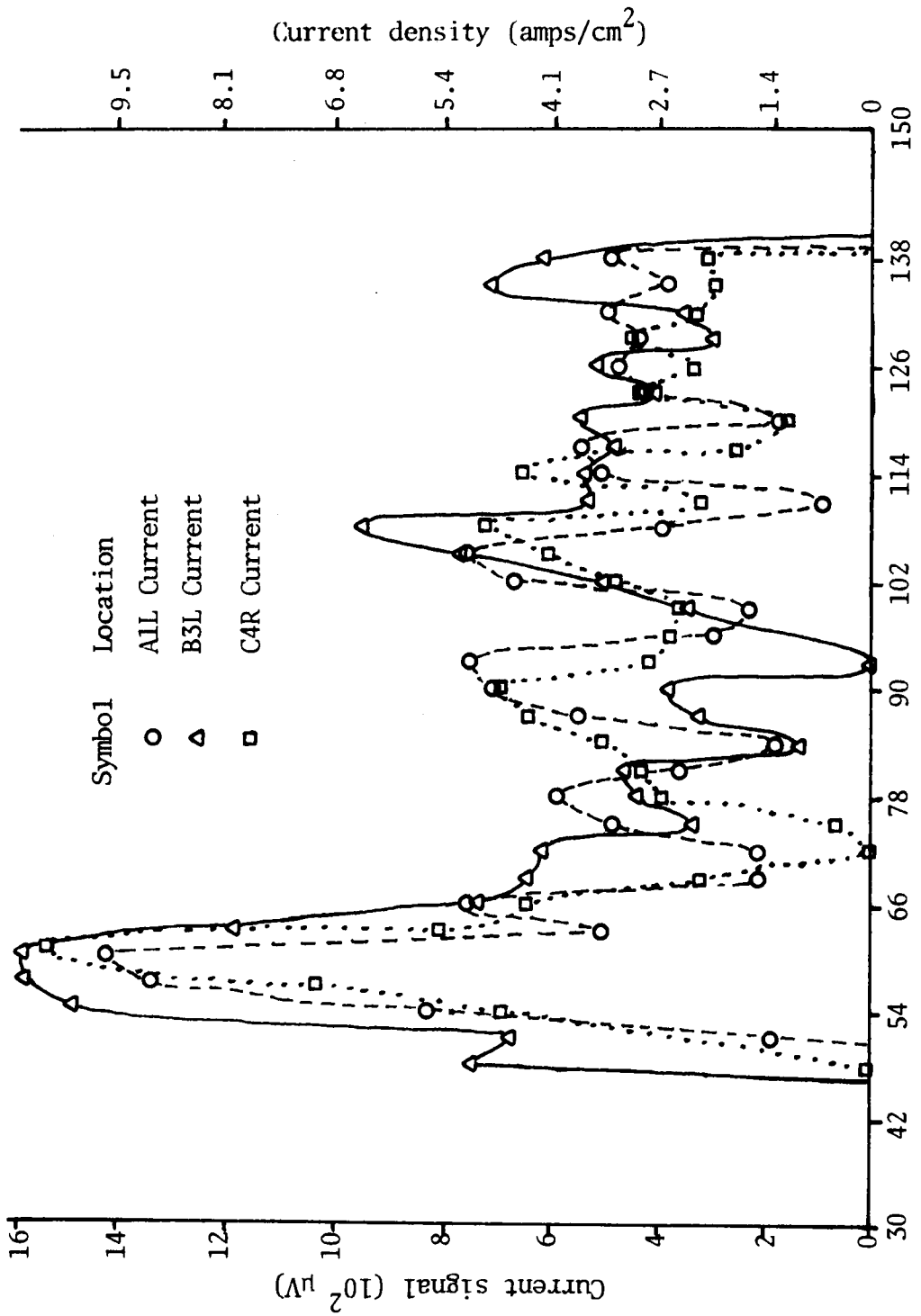



Figure 17. Current density versus time for segments on run number 1483.

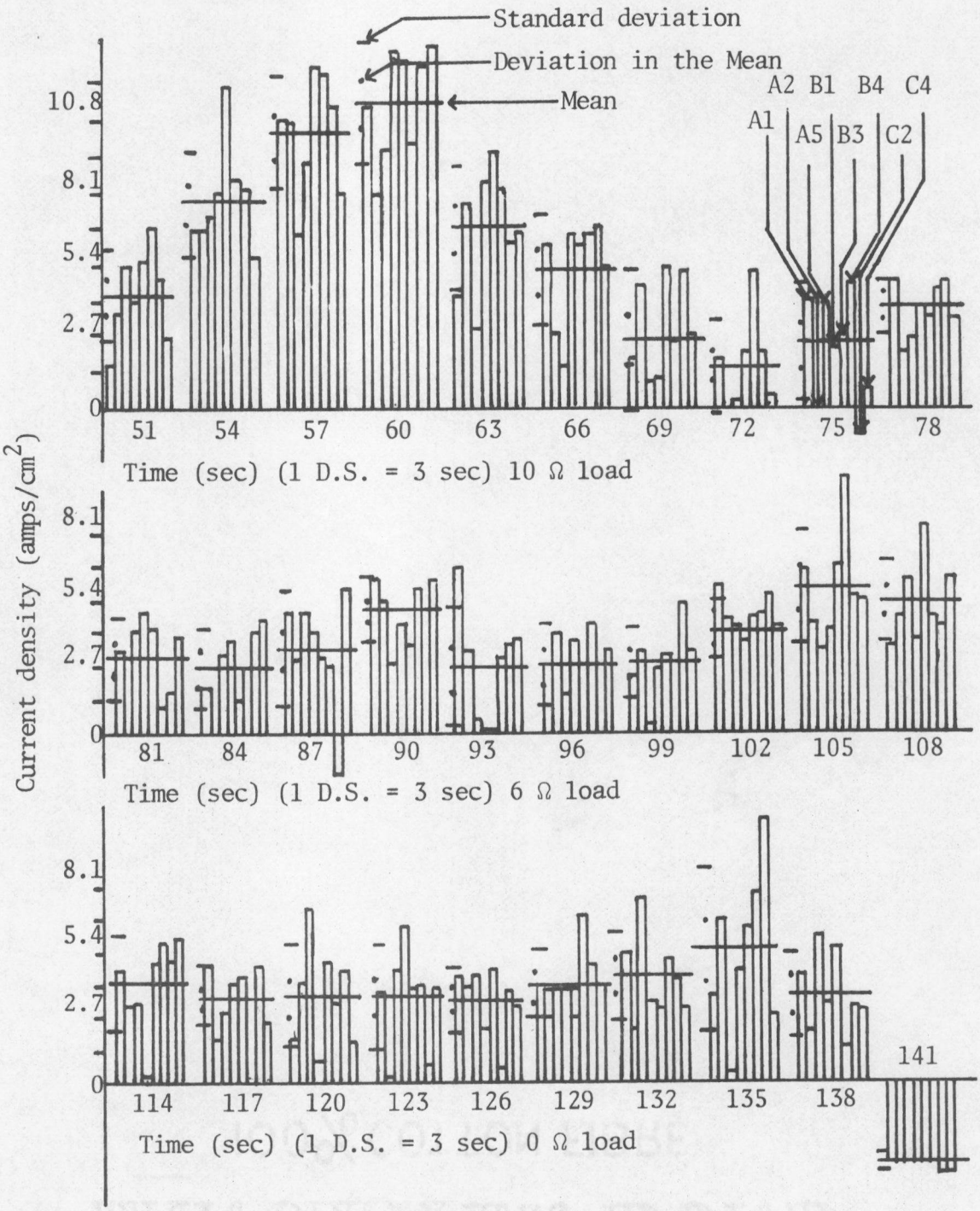



Figure 18. Current histogram showing the mean, standard deviation, and deviation in the mean taken for each data set for run number 1483.

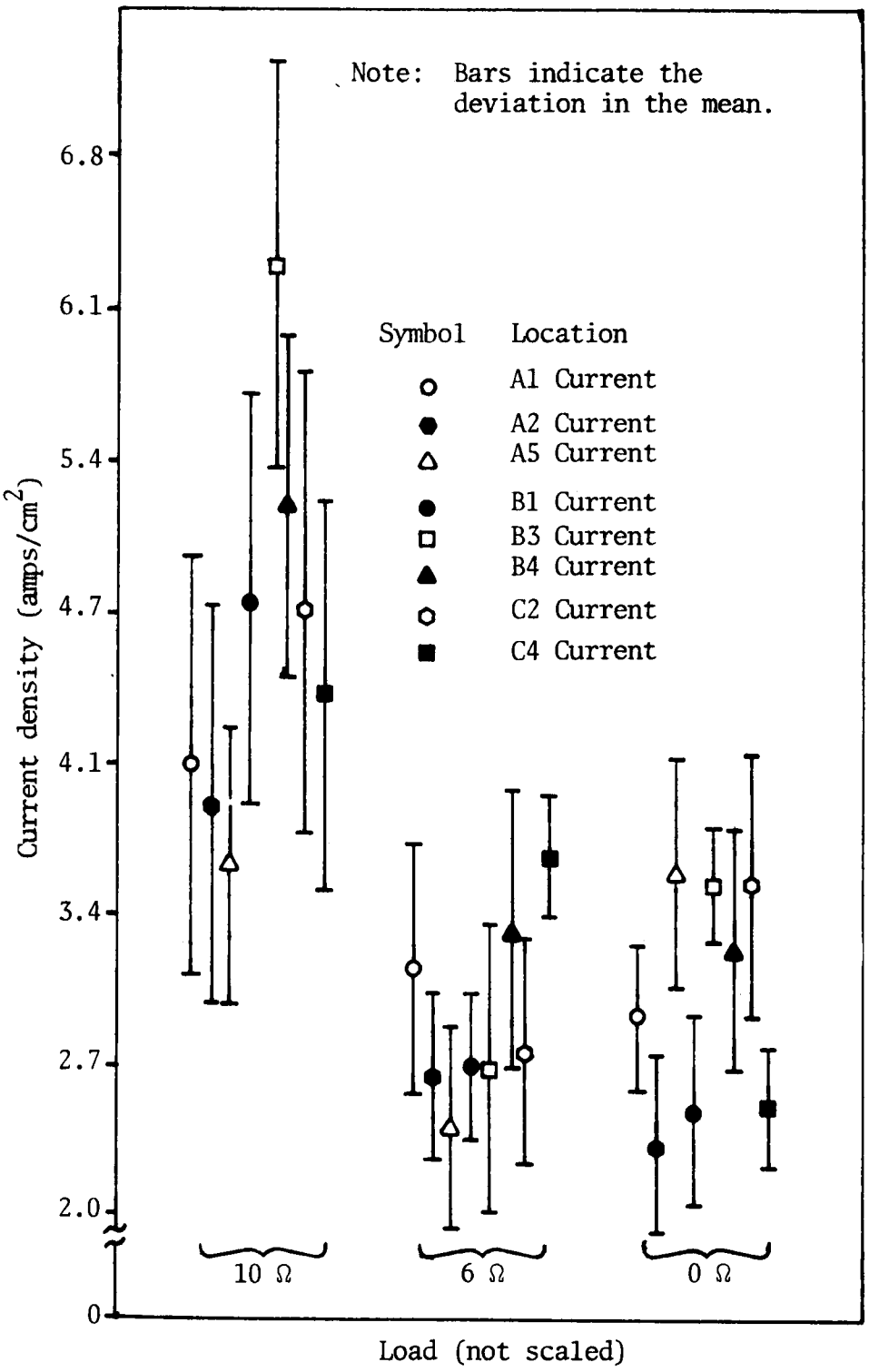



Figure 19. Time-averaged current density for each segment and at each load on run number 1483.

leaks were apparently stopped. The surface temperature was of the order of 1,000 C. As is shown in Figure 20, thermal equilibrium was not reached during the two minutes of combustion.

Discussion of Data on Run Number 1487

Figure 21 shows the histogram of current segments that were still in operation. The signal is clearly dependent upon time with little obvious position dependence. This is illustrated in Figure 22. Segment B3 in the center of the electrode was instrumented to be read nine times during each data set. The time between each B3 reading was about 120 milliseconds. The solid bars in Figure 22 indicate the times that the other segments were read with respect to the nearest B3 reading and show also the relative magnitudes. It is evident then that the segments went up and down in their conduction together. The data is plotted chronologically.

Figure 23 shows the average over time of the different segments. The error bars are the deviation in the means. These are as large as they are because the current in the generator is unsteady.

A statistical analysis was also made using the Chi-squared goodness of fit test. The number of values of the signal levels were taken lying outside the region $\overline{X} \pm \sigma$ where X-bar was the signal average over space of a data set and Sigma was the standard deviation. These values were

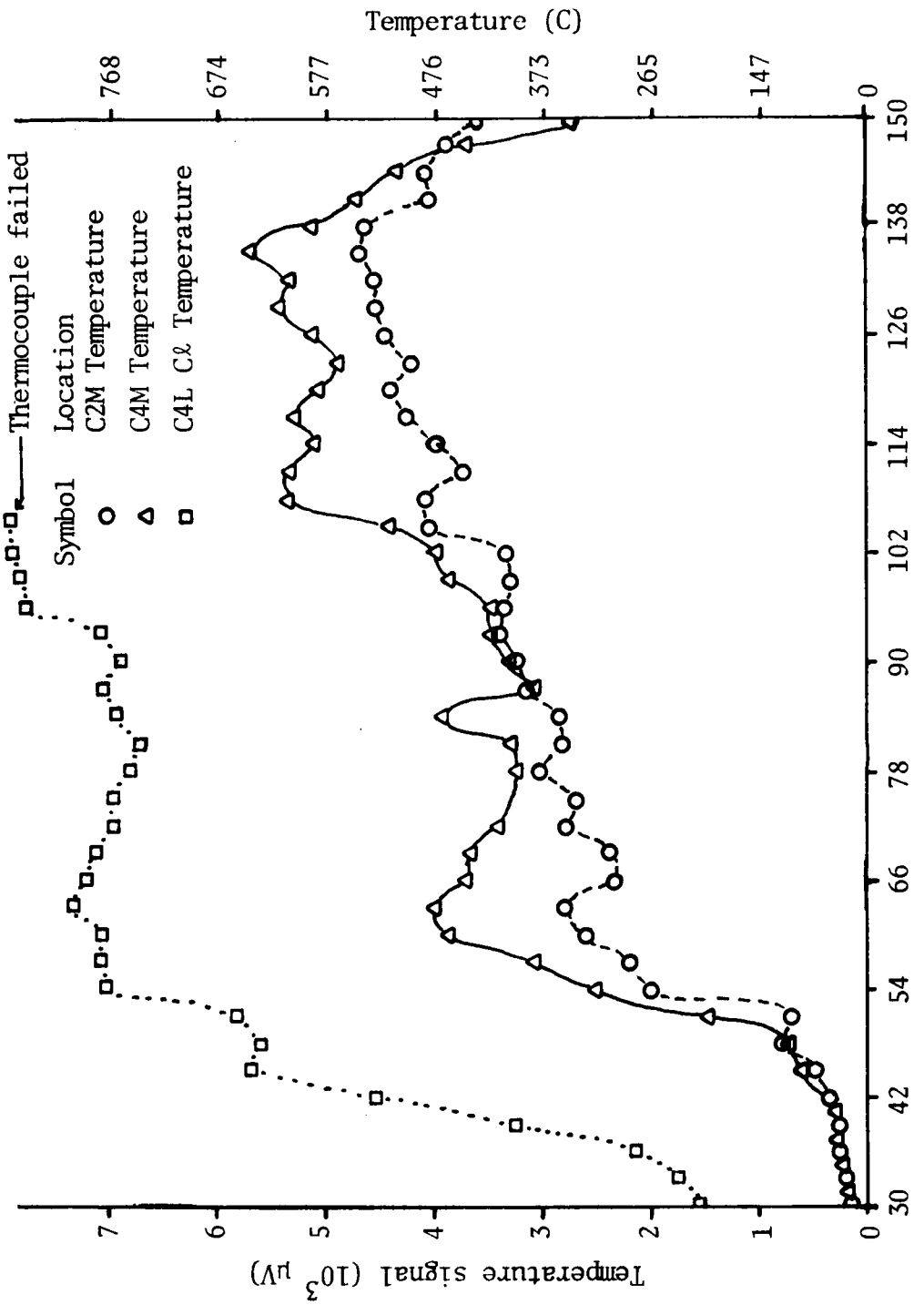



Figure 20. Temperature history of run number 1483.

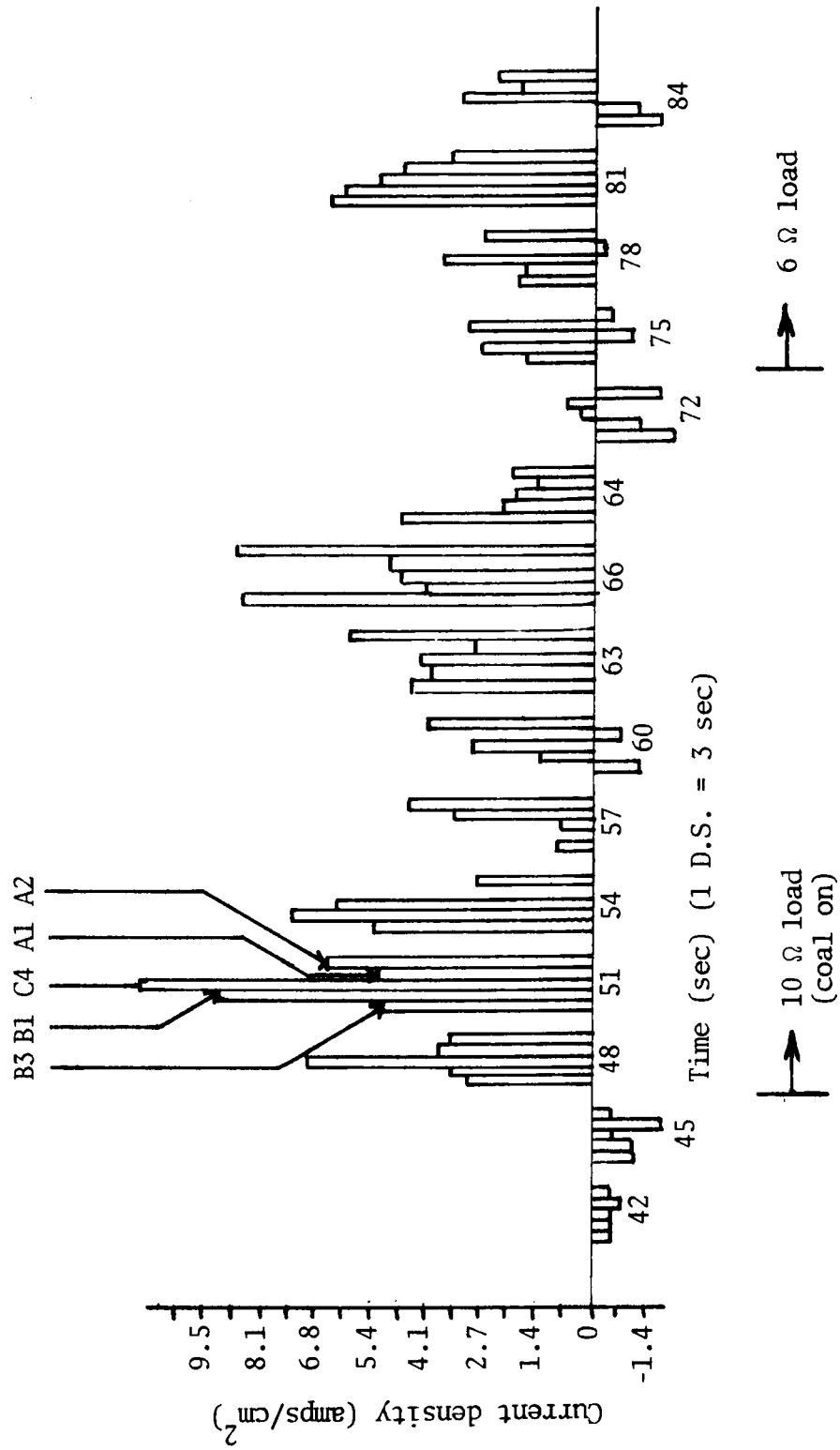



Figure 21. Current density histogram for segments on run number 1487.

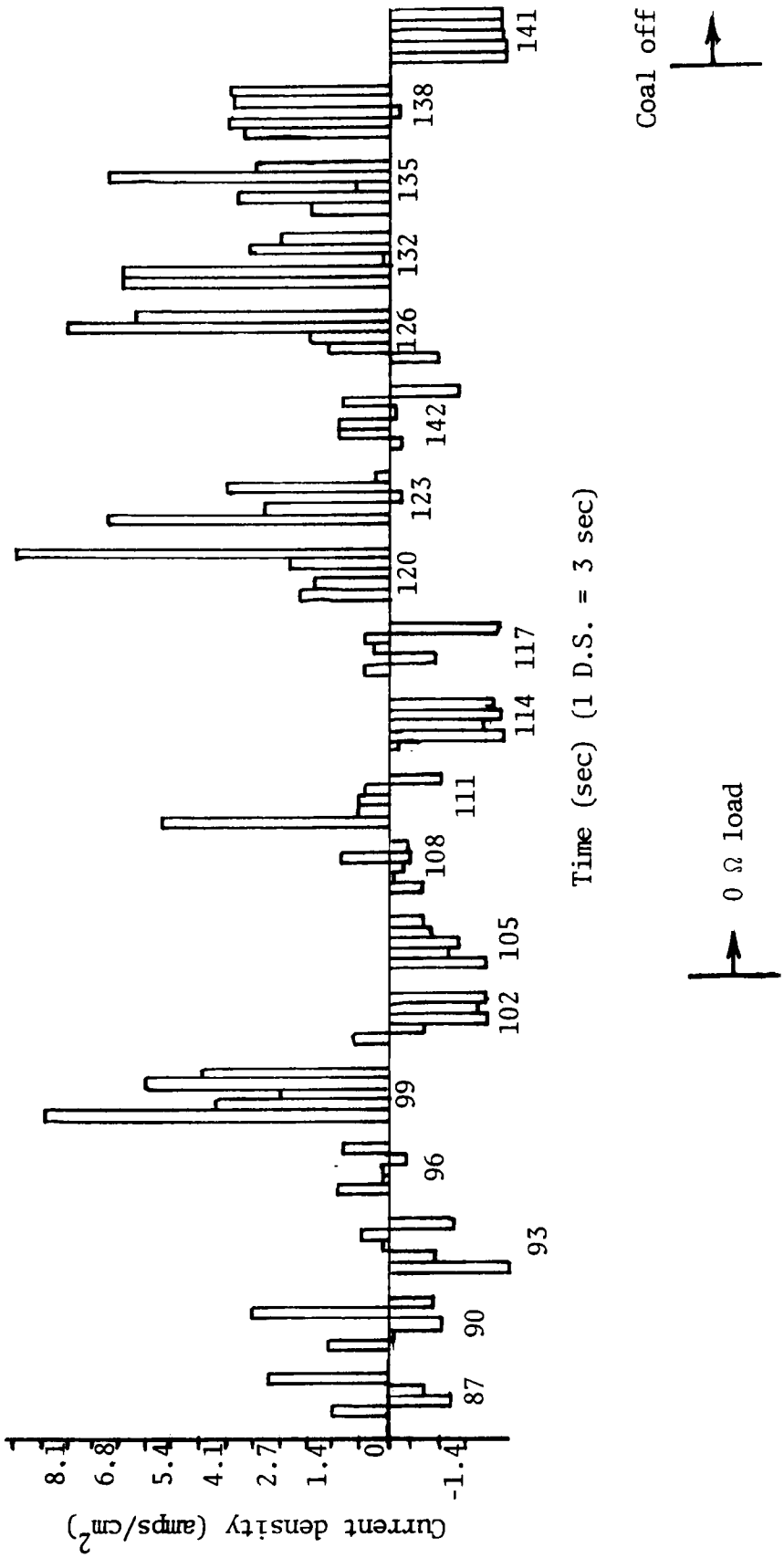



Figure 21. (continued)

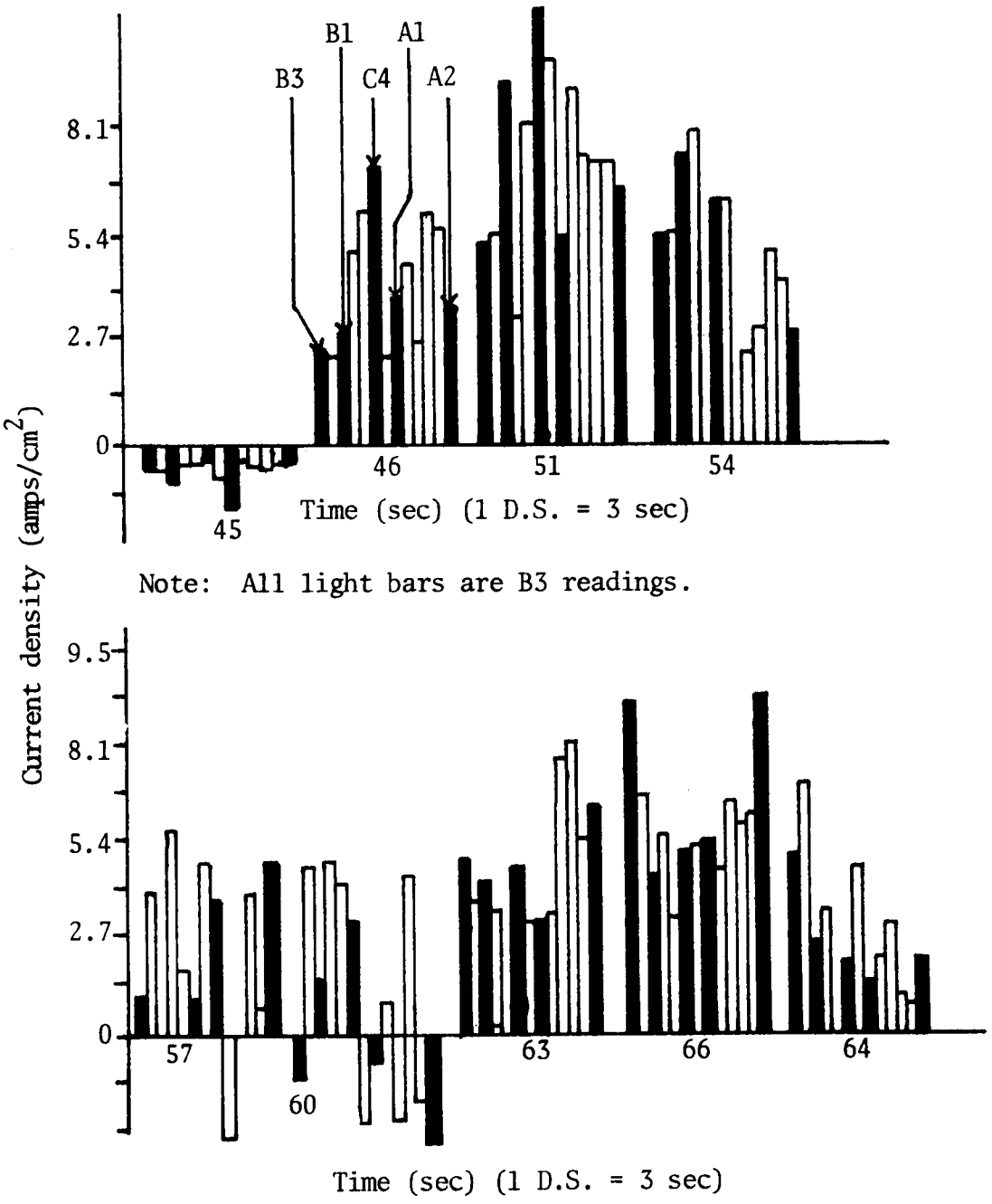



Figure 22. Current density histogram with B3 segment read several times during each data set for run number 1487.

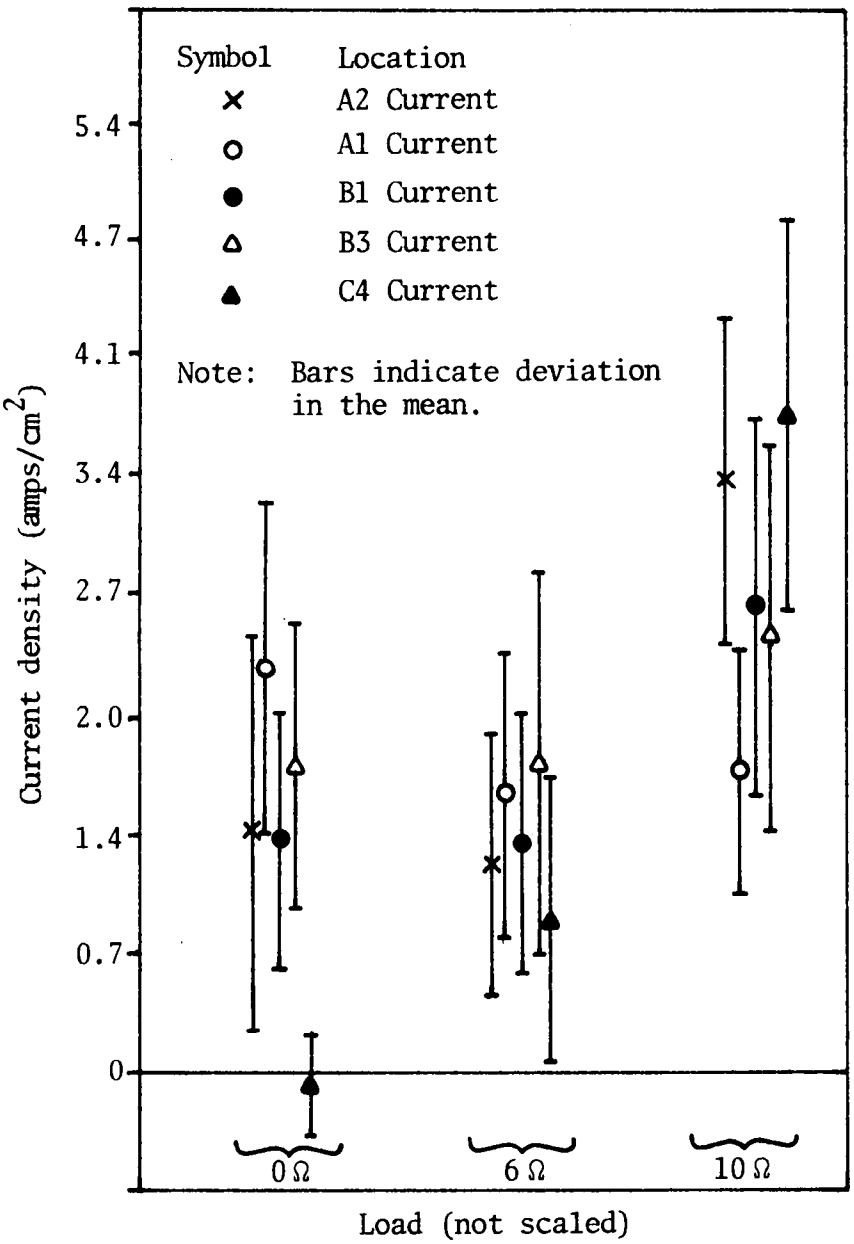



Figure 23. Time-averaged current density on run number 1487 for each segment and load.

found to be evenly distributed among the segments. That is, the current did not prefer any particular segment.

A slightly different method of analysis is represented by Figures 24, 25, and 26. They present the current distributions under the loads of 10 ohms, 6 ohms, and zero ohm. The height of the bars represents the current density of a particular segment averaged over the length of time that the indicated load was applied.

Finally, assume a thermal emf effect of about 2.7 amps/$cm^2$, as seen in data set 47 on Figure 21, and obtain a 1.4 amps/$cm^2$ current density from Figure 23 for the zero ohm case. Adding the two gives an observed current density of 4.1 amps/$cm^2$. Such a figure appears to be higher than previous work has indicated. Another difficulty that requires explanation is the following. Even though current concentration was not observed in any of the second series of tests, noticeable erosion had occurred near C2 and C5. Unfortunately, no instrumentation had been applied where the erosion took place.

A post-test experiment was made where the electrode was calibrated at high current. The electrode showed current distribution similar to Figure 24 when the current was concentrated in the eroded places. About 4 amps gave these readings. This corresponds to 0.3 amp/$cm^2$ if this current is averaged over the entire Inconel electrode. Stephan's work is within a factor of three.

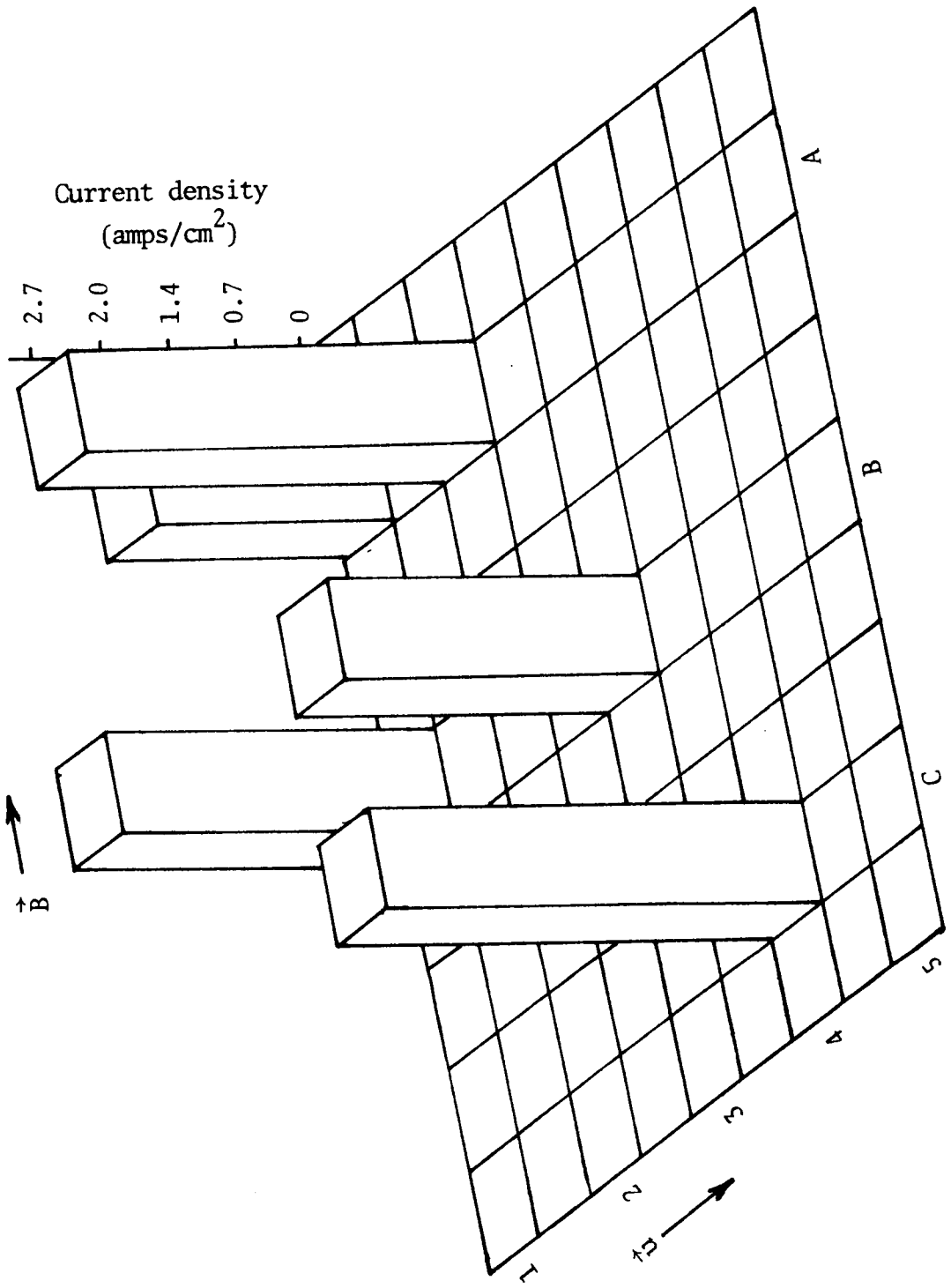



Figure 24. Time-averaged current density as a function of position for run number 1487 at 10-ohm load.

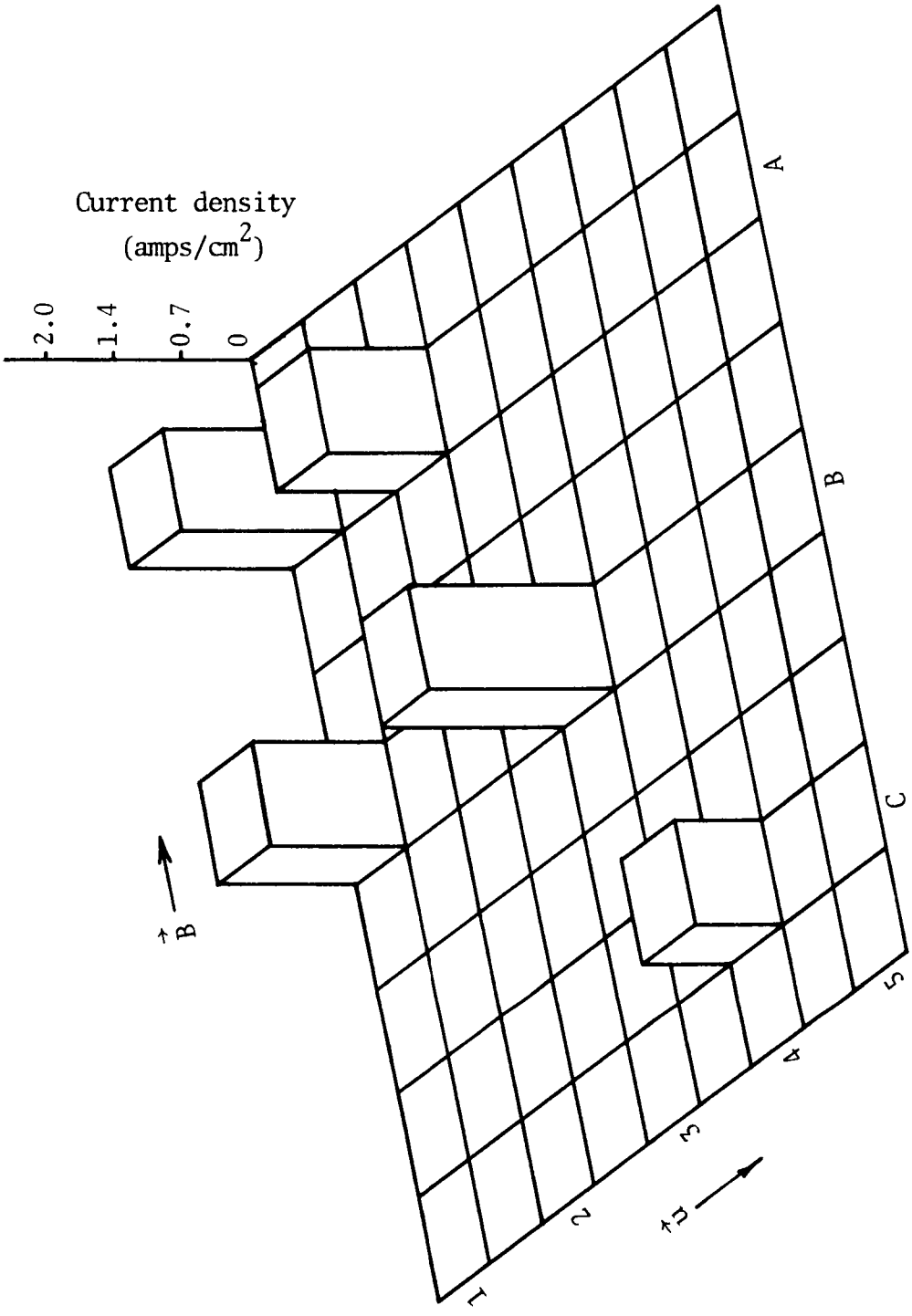



Figure 25. Time-averaged current density as a function of position for run number 1487 at 6-ohm load.

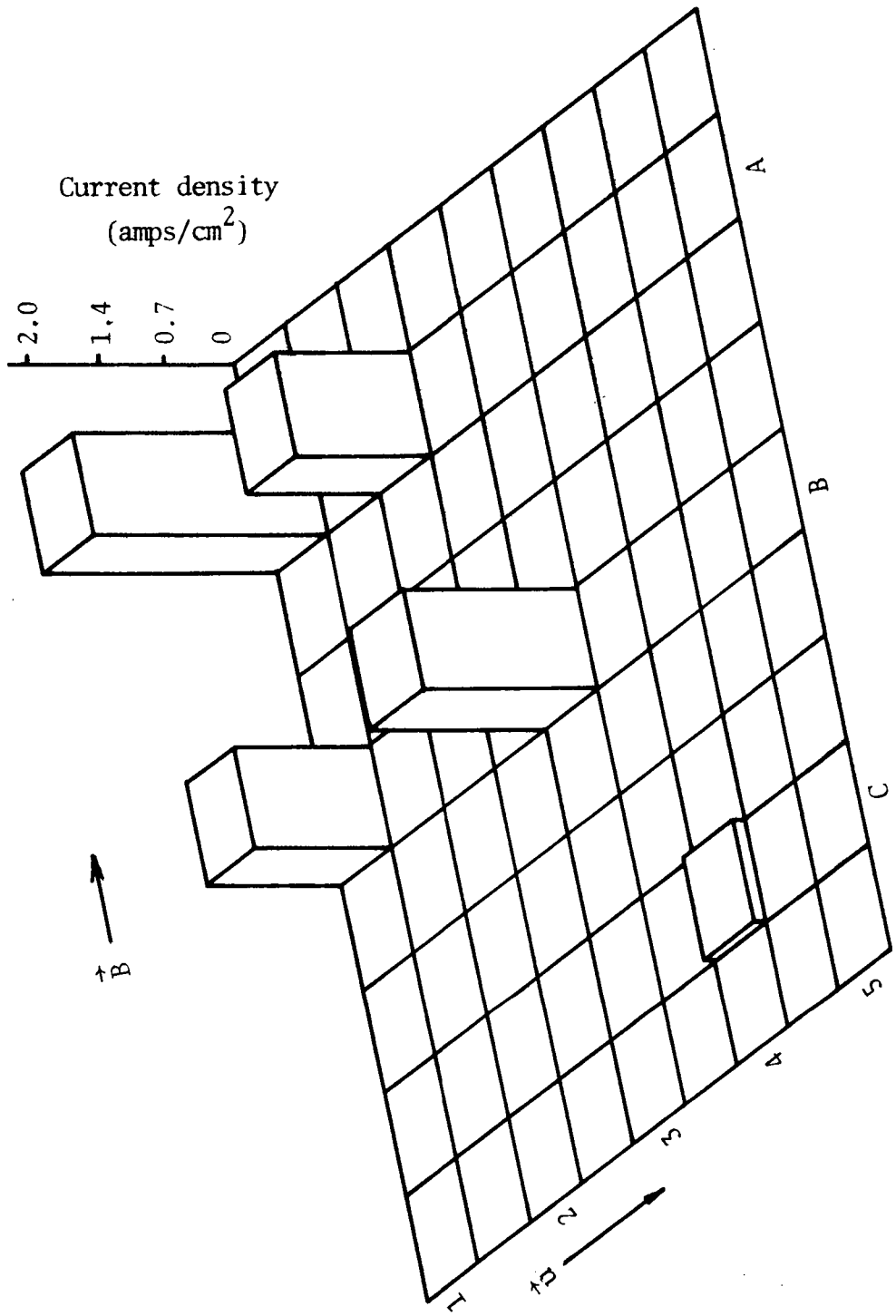



Figure 26. Time-averaged current density as a function of position for run number 1487 at zero-ohm load.

Cross talk had increased only a few percent and the post-test calibration was also within a few percent. Linearity was good from 5 milliamps to 25 amps. A cross talk signal from a current concentration near the eroded areas gives roughly the observed signals.

Two difficulties still remain. A distribution with C4 low, as shown in Figure 26, is not obtainable from the current concentration hypothesis. Therefore, Figures 24, 25, and 26 must represent some part of what the current distribution is doing. The other difficulty with current concentration has to do with the nature of the anode voltage drop. As was shown by Nicholson [5], the resistive character is positive. Thus, for an increase in current density, the resistance in the anode drop would go up. The current, however, will seek a lower resistive path so that the current density would ultimately be redistributed and come back down.

## Comparison with Conformal Mapping Theory

Calculations were made using the theory for the axial direction only, when y, the distance above the electrode, was set to zero. The equations were simplified considerably with this condition. Further, the current density at the surface was the primary interest.

Table 4 lists the physical parameters needed to solve the equations. The total generator current I was taken from oscillograph data on run number 1487 when the

Table 4

Generator and Plasma Parameters Needed for Current Density Calculation

| Generator Parameter | Plasma Parameter |
|---|---|
| $d = 18.5$ cm | $\varepsilon = 0.726$ rad. |
| $D = 5.05$ cm | $k = 0.169$ |
| $A = 93.8$ cm$^2$ | $1-k = 0.831$ |
| $c = 0.9689$ | $I = 66$ amps |
| $c' = 0.0311$ | $\Omega = 1.7$ |
| $2\rho = 3.22$ cm | |
| $a_o = 1.61$ cm | |
| $u(c) = 1.25$ | |
| $u'(c') = 0.025$ | |
| $v(c) = 0.70$ | |
| $v'(c') < 0.005$ | |

load was 10 ohms. At high loads the DCW generator corresponds closely to the Faraday generator. The theory was developed for the Faraday mode.

Figure 27 shows the comparison of experimental current distribution with the theoretical calculation from Eq. (4). The theoretical current distribution is calculated along the x direction by computer. The dashed line on Figure 27 represents the average current density over the entire electrode for run number 1487 at 10 ohms load. After determining the experimental average, the theoretical curve is normalized so that the area under it is the same as under the experimental average curve.

As can be seen, the data does not agree with the theoretically calculated current distribution particularly on the upstream edge, i.e., when x is small. Further, the current density does not appear to be reduced on the downstream edge.

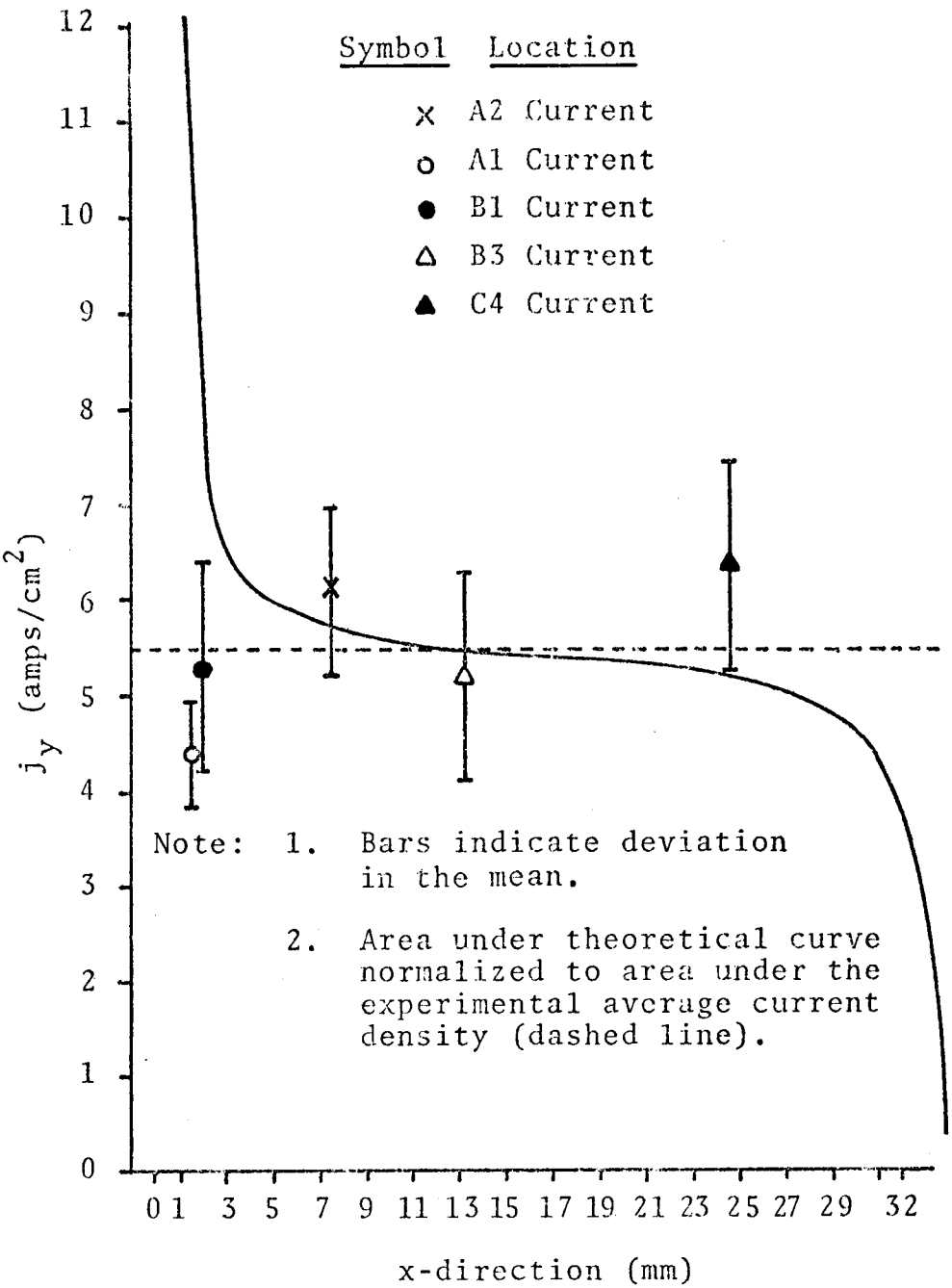



Figure 27. Comparison of experimental and theoretical current distribution on the anode on run number 1487 and at 10Ω load.

# CHAPTER IV

## CONCLUSIONS AND RECOMMENDATIONS

Qualitatively, the current fluctuations on an electrode have been observed during the course of a run. The time resolution is of the order of one second if the B3 data is used. Spatially, it is necessary to take a time average and compare "patterns," as in Figures 24, 25, and 26, pages 59, 60, and 61, respectively, in order to obtain current distribution. This would be a very useful technique if some type of automated display was available. When current concentration was extensive, as in run number 1482, there was a noticeable increase in temperature at the surface and inside the electrode.

Quantitatively, the results are in question. Current concentration was certainly observed on the anode in the first test. The magnitude measured is possible and probably correct. For the other tests, however, there was erosion, no observed current concentration, and too high a current density if the data is interpreted without current concentration.

The root of the problem lies in the design. If instrumentation had been applied to every segment, the question of current concentration in the later tests would be resolved. A further recommendation is to design the electrode so that the probe wires are not in the slots.

When the alumina insulation erodes, the wires are exposed and have a higher probability of failure. Finally, the cooling water should not have a path to the plasma. If probe intrusion into the water passage is unavoidable, the sealing material and technique should be tested under generator conditions.

# BIBLIOGRAPHY

# BIBLIOGRAPHY


1. Hurwitz, H., Jr., R. W. Kilb, and G. W. Sutton. "Influence of Tensor Conductivity on Current Distribution in a MHD Generator," Journal of Applied Physics, 32:205, February, 1961.

2. Oliver, D. A., and M. Mitchner. "Nonuniform Electrical Conduction in MHD Channels," AIAA Journal, 5:1424, August, 1967.

3. Maxwell, C. A., S. T. Demetriades, and S. R. Davis. "Resistive Coatings over MHD Electrodes-Theoretical and Experimental Studies." Paper presented at the Fourteenth Symposium on Engineering Aspects of MHD, The University of Tennessee Space Institute, Tullahoma, Tennessee, April, 1974.

4. Taylor, R. E., Y. C. L. Wu, and D. L. Denzel. "Effects of Boundary Layers Upon Current Distribution and Internal Resistance in Segmented Magnetohydrodynamic Channels," Journal of Applied Physics, 42:2689, June, 1971.

5. Nicholson, M. K. "Current Distribution and Electrode Voltage Drop Effects in a Diagonal Wall MHD Generator." Unpublished Master's thesis, The University of Tennessee, Knoxville, 1972.

6. Martin, J. F. "Current Distribution in a Hall Generator Electrode." Unpublished Master's thesis, The University of Tennessee, Knoxville, 1970.

7. Stephans, J. N. "An Experimental and Theoretical Study of an Electrode Immersed in a Moving Plasma with an Externally Applied Magnetic Field." Unpublished Master's thesis, The University of Tennessee, Knoxville, 1970.

8. Finkelburg, W., and H. Maecker. Handbuch der Physic. Berlin: Springer-Verlag, 1956.

9. Muehlhauser, J. W. "Analytical and Experimental Studies of Electrical Discharges on Cathode Surfaces of a MHD Generator." Ph.D. dissertation, The University of Tennessee, Knoxville, 1974.

10. Wu, Y. C. L., D. L. Denzel, S. Witkowski, R. V. Shanklin, III, U. Zitzow, J. Muehlhauser, P. Chang, E. S. Jett, and J. B. Dicks. "Two-Terminal Connected Open-cycle MHD Generators." Paper presented at the Ninth Symposium on Engineering Aspects of MHD, The University of Tennessee Space Institute, Tullahoma, Tennessee, April, 1968.

11. Inconel Alloy 625. Huntington, West Virginia: Huntington Alloys, Inc., 1966.

# VITA

Glen Arthur Kroeger was born in Hays, Kansas, September 15, 1947. He attended Washington Elementary School and Ellis High School, Ellis, Kansas, graduating valedictorian in 1965. Entering Midland Lutheran College, Fremont, Nebraska, in the fall of the same year, he graduated in 1969 receiving a Bachelor of Arts degree with a major in physics and a minor in mathematics. In August, 1969, he enlisted in the United States Air Force and served four years as an electronics technician. One Southeast Asian tour in Thailand was served. Following discharge, he entered The University of Tennessee Space Institute in the fall of 1973. He graduated with a Master of Science degree with a major in physics in the spring of 1976. He is a member of Blue Key National Honor Fraternity and the American Association of Physics Teachers.